LHCb-PUB-2018-015
February 14, 2019

Physics opportunities with the fixed-target program of the LHCb experiment using an unpolarized gas target

A. Bursche[1], H. Dembinski[2], P. Di Nezza[3], M. Ferro-Luzzi[4], F. Fleuret[5,6], G. Graziani[7], G. Manca[1,8], E. Maurice[5,6], N. Neri[9,10], L. Pappalardo[11,12], P. Robbe[5], M. Schmelling[2], M. Winn[5], V. Zhukov[13,14]

[1] *INFN Sezione di Cagliari, Monserrato, Italy*
[2] *Max-Planck-Institut für Kernphysik (MPIK), Heidelberg, Germany*
[3] *INFN Laboratori Nazionali di Frascati, Frascati, Italy*
[4] *European Organization for Nuclear Research (CERN), Geneva, Switzerland*
[5] *LAL, Univ. Paris-Sud, CNRS/IN2P3, Université Paris-Saclay, Orsay, France*
[6] *Laboratoire Leprince-Ringuet, Palaiseau, France*
[7] *INFN Sezione di Firenze, Firenze, Italy*
[8] *Università di Cagliari, Cagliari, Italy*
[9] *INFN Sezione di Milano, Milano, Italy*
[10] *Università degli Studi di Milano, Milano, Italy*
[11] *INFN Sezione di Ferrara, Ferrara, Italy*
[12] *Università di Ferrara, Ferrara, Italy*
[13] *I. Physikalisches Institut, RWTH Aachen University, Aachen, Germany*
[14] *Institute of Nuclear Physics, Moscow State University (SINP MSU), Moscow, Russia*

Abstract

The LHCb experiment pioneered fixed-target physics with LHC beams, thanks to the SMOG internal gas target. Collisions of proton and heavy-ion beams on targets with different nuclear size can be recorded at a centre-of-mass energy of $\sqrt{s_{\rm NN}} \sim 100$ GeV. This note summarizes the physics opportunities offered by the current fixed-target setup and its upgrade envisaged for the LHC Run 3. Unique measurements are being performed with Run 2 data, covering in particular heavy flavour production in nuclear collisions over a wide Feynman-x range and light particle production of particular interest to cosmic ray physics. The increase in luminosity and extension of the choice of target material, which are being pursued for Run 3, open many new possibilities which are reviewed in this document.

1 Introduction

The physics case for a fixed-target experiment exploiting the unprecedented energy of the LHC beams has been advocated since several years, notably by the AFTER initiative [1–3], though no dedicated lines to extract the beam for such an experiment have been foreseen so far in the LHC accelerator complex.

The LHCb experiment developed an internal gas target offering the possibility to study beam-gas collisions with negligible effect on LHC operations. The device, named SMOG (System for Measuring Overlap with Gas) [4], was originally conceived to allow for a novel beam imaging technique using beam-gas collisions [5], which was successfully used to determine the luminosity of pp collisions at the LHC with unrivaled accuracy [6].

Through the SMOG device, noble gases (presently helium, neon and argon) can be injected inside the LHC vacuum pipe in the proximity of the LHCb collision point at a nominal pressure of about 2×10^{-7} mbar. For a LHC beam of 10^{14} protons, this corresponds to a luminosity of $6 \times 10^{29}\text{cm}^{-2}\text{s}^{-1}$ for collisions occurring in one meter of gas along the beam direction, which is roughly the acceptance of the LHCb vertex detector. The potential for unique physics measurements offered by such collision rate, combined with the LHCb specific capabilities for reconstruction and identification of particles produced in the forward direction, was soon recognised [7].

Collisions of LHC beams on fixed targets enable to study production of particles carrying a large momentum fraction of the target nucleon in the nucleon-nucleon center-of-mass (c.m.) frame, at an energy scale up to 115 GeV. Another advantage of the fixed-target configuration over the beam-beam setup is the wider choice of the collision system, providing novel probes for the study of nucleon and nuclear structures, and measurements of great interest to cosmic-ray physics.

This note summarizes the physics opportunities achievable by this program using the data samples collected during the LHC Run 2, and the measurements achievable during Run 3 after improving the target both in terms of achievable gas density and wider choice of the target gas. The current setup of LHCb in its fixed-target mode and the proposed target development, named SMOG2, are discussed in Section 2. Section 3 summarizes the experience gained with data taking of beam-gas collisions performed during Run 2, discussing the experimental challenges and the benefits that are expected from the target upgrade. A possible scenario for the future data taking with SMOG2 is discussed in Section 4.

Status and prospects for measurements related to heavy ion physics (Section 5), hadron production and cosmic ray physics (Section 6), and nucleon structure (Section 7) are then discussed, stressing the unique contributions achievable in the worldwide context.

2 Experimental setup

The LHCb detector is a single-arm forward spectrometer, sketched in Figure 1, covering the pseudorapidity range $2 < \eta < 5$ and whose layout and performance are described in detail in Refs. [8, 9]. The forward geometry is particularly well suited to the study of beam-gas collisions.

With the vertex locator (VELO) the precise position of the interaction vertex can be determined for collisions occurring in a region of about one meter length along the

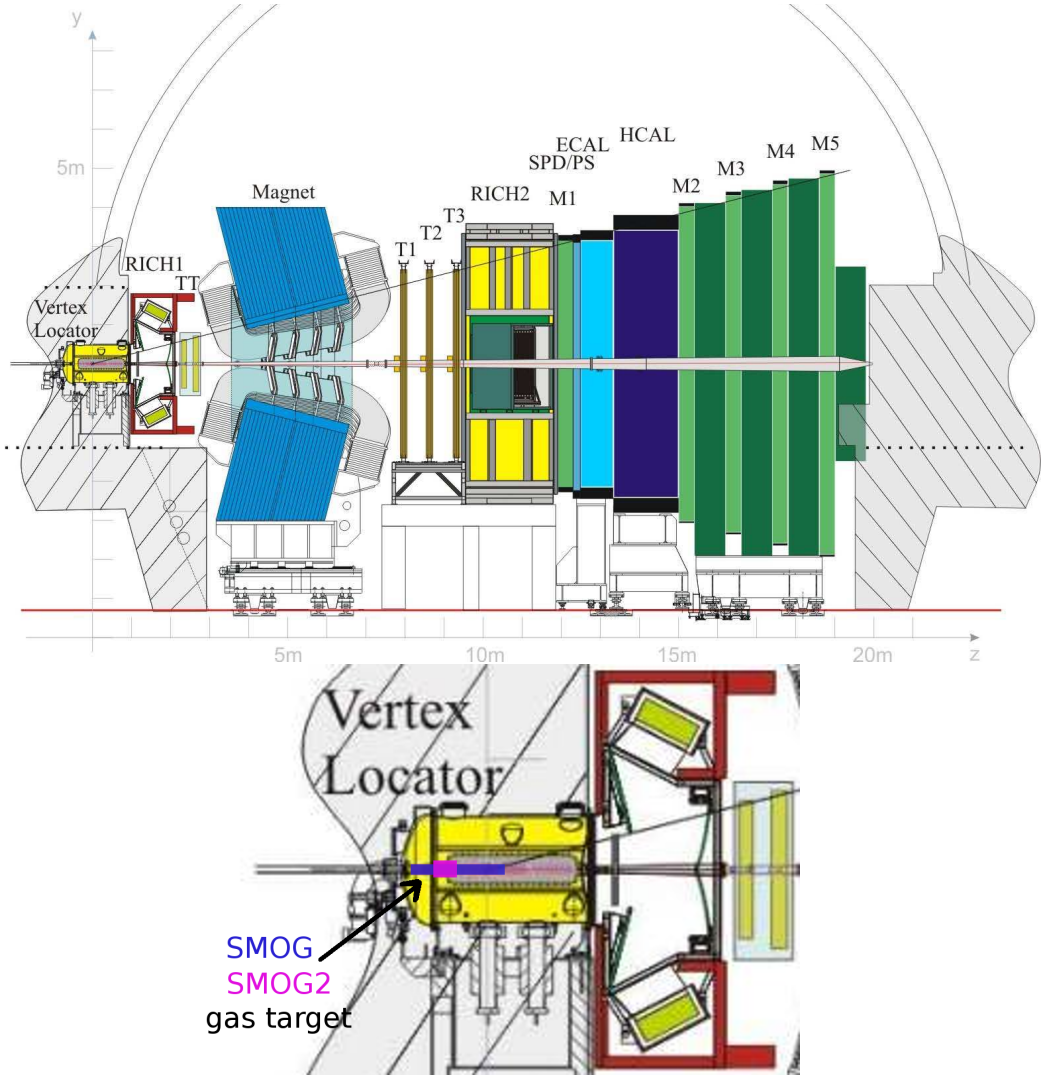

Figure 1: The upper drawing shows the layout of the LHCb experiment. In the bottom drawing, the vertex locator region is zoomed, showing the spatial extension of the internal gas target, provided by the SMOG device, currently exploited for physics measurements, as well as that of the proposed SMOG2 target, discussed in Section 2.2.

beam direction, and secondary vertices from heavy flavour decays can be reconstructed. Charged particles are reconstructed by the tracking system with a relative uncertainty on their momentum, p, that varies from 0.5% at low momentum to 1.0% at 200 GeV/c. The covered η range is fully instrumented with two ring-imaging Cherenkov detectors (RICH), a calorimeter system and a muon system, allowing to distinguish different types of charged particles in the momentum range from about 2 to 100 GeV/c (proton/kaon separation is achievable from about 10 GeV/c). The calorimeter system consists of scintillating-pad (SPD) and preshower detectors, an electromagnetic calorimeter (ECAL) and a hadronic calorimeter (HCAL), also providing reconstruction/identification capabilities for neutral particles.

In the fixed-target configuration, proton or ion beams with energy per nucleon $E_{\rm N}$ between 0.9 and 7 TeV give rise to nucleon-nucleon collisions with a centre-of-mass (c.m.) energy $\sqrt{s_{\rm NN}} \sim \sqrt{2E_{\rm N}M_{\rm N}}$ between 41 and 115 GeV. The corresponding rapidity of the

c.m. frame $y_{CM} \sim \text{arcsinh}(\sqrt{E_N/(2M_N)})$ varies between 3.8 and 4.8, implying that the LHCb acceptance covers particles produced at central and backward rapidities in the c.m. frame. This allows to observe particles carrying a large fraction of the initial longitudinal momentum of the target nucleon in the c.m. frame, usually expressed through the Feynman-x variable

$$x_F \equiv \frac{p_L^*}{|\max(p_L^*)|} \simeq \frac{2}{\sqrt{s_{\rm NN}}}\sqrt{M^2+p_{\rm T}^2}\ \sinh(y^*),$$

where M is the particle mass, $p_{\rm T}$ its transverse momentum, p_L^* and y^* the longitudinal momentum and rapidity in the c.m. frame. As an example, for the Run2 beam energy of 6.5 TeV, x_F up to -0.5 for J/ψ and -1 for $\Upsilon(1S)$ can be observed in fixed-target configuration. The Feynman-x variable is related to the Bjorken-x variable of the two colliding partons as $x_F \sim x_1 - x_2$, hence a large negative x_F value corresponds to large Bjorken-x values in the target nucleon, which are accessible in beam-beam collisions only at much larger Q^2, as illustrated in Figure 2.

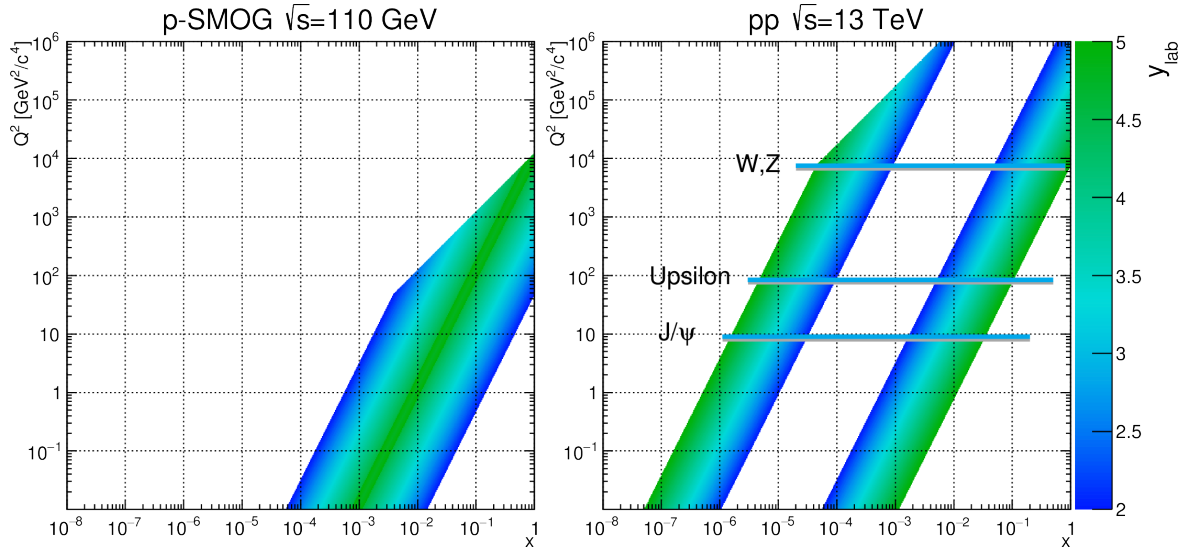

Figure 2: Accessible range in the (x, Q^2) plane in (left) the fixed-target (SMOG) configuration, compared to (right) the collider configuration at LHCb.

2.1 Current fixed-target layout

The SMOG device [4,6] allows the injection of noble gases in the beam pipe section crossing the VELO region, providing the possibility to operate LHCb as a fixed-target experiment. When the SMOG device is used, the two ion pumps of the VELO vacuum system are switched off. A valve is opened which connects the VELO to an auxiliary volume where gas flows into a turbo-molecular pump at a stable pressure. The gas can flow into the beam pipe toward the closest vacuum pumps, located about ± 20 m away from the nominal LHCb collision point. The gas species which are compatible with the LHC vacuum system in this configuration are presently limited to helium, neon and argon. The gas pressure in the VELO region is of order 10^{-7} mbar, which is small enough not to significantly perturb the LHC operation. The injected gas pressure can be monitored by four cold-cathode

gauges (Penning type) and one hot filament ionization gauge (Bayard-Alpert type) located at various positions around the VELO. The absolute calibration of the cold-cathode gauges exhibits a variation at ±50% level. The calibrated ionization gauge was installed early 2017, at about $z = -7$ m, and could be used in combination with molecular flow simulations to quantify the density in the VELO vacuum at the +/-20% level of accuracy.

2.2 Proposed target upgrade

The LHCb detector will undergo a major upgrade in view of the LHC Run 3, which is planned to start in 2021 [10]. As the goal is to be able to run in *pp* collisions at increased instantaneous luminosity, the whole tracking system, notably the VELO detector [11], has been redesigned with a finer granularity. The detector performance for fixed-target collisions is thus expected to be further improved, at least for events acquired in low pile-up conditions.

An improved design for the gas target, called SMOG2, has been recently proposed [12] and approved by the LHCb collaboration to be integrated in the design of the upgraded VELO detector [13]. In this new design, the gas would be contained in a storage cell, illustrated in Figure 3. The cell consists of a 20 cm long tube with a diameter of 1 cm, fed by a capillary tube. The target is placed 40 ± 10 cm upstream of the nominal LHCb collision point. The cell is made from two halves which, as the rest of the VELO detector, can be retracted from their operating position while the LHC beams are being injected and tuned, and closed when stable beams are declared. Outside the open ends of the cell, the gas density is suppressed by the VELO vacuum pumps, so that the beam-gas collisions occur mostly inside the cell. This allows to increase the effective areal density in the target by up to two orders of magnitudes with respect to SMOG for the same gas flow. Even higher densities could be considered if compatible with the spectrometer occupancy and machine operation.

In this configuration, the use of more gas species, notably H_2 and D_2, and heavier noble gases (Kr, Xe) could become possible. The device will be equipped with a more sophisticated Gas Feed System. This, combining the possibility to measure both the gas flow and the cell temperature precisely, will allow for a significantly more precise determination of the target density (and luminosity), reaching the level of few percent accuracy.

Also worth mentioning is the possibility to exploit all circulating bunches for fixed-target physics, i.e. to run simultaneously in fixed-target and in collider mode, thanks to the limited extension of the SMOG2 target region, not overlapping the *pp* interaction region. This is possible if the beam-gas interactions generate tolerable background to the mainstream *pp* physics program and vice versa.

On a longer time scale (Run 4/Run 5), more ambitious proposals for target upgrades are also being considered:

- a polarized gas target, to be installed upstream of the VELO (LHCSpin initiative [12]);
- an off-axis solid target coupled to a bent crystal, hit by a secondary proton beam, allowing to measure the magnetic and electric dipole moments (MDM/EDM) of heavy baryons and possibly τ leptons [14–19];

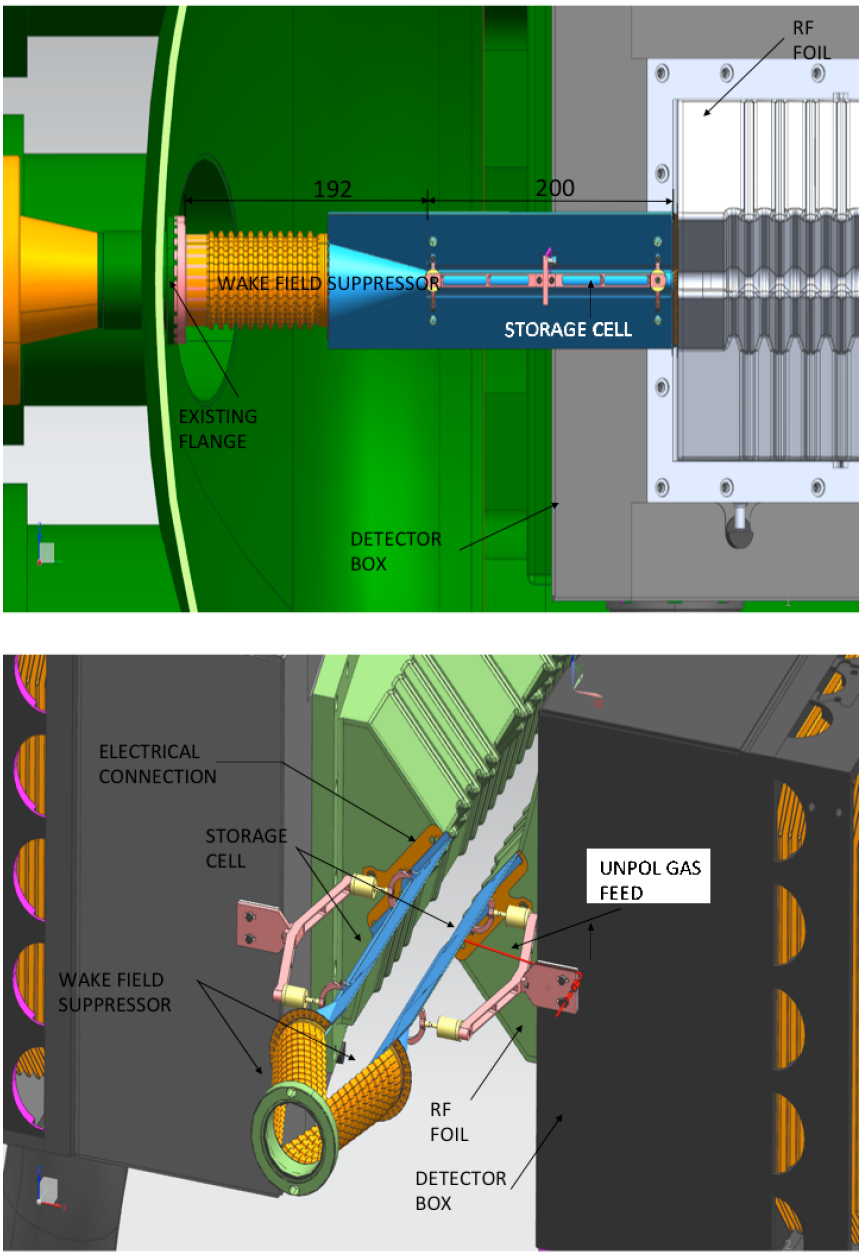

Figure 3: Proposed layout of the SMOG2 gas target. The upper sketch illustrates the storage cell in its operating (closed) position. In the events of interest, the beam crosses the cell from left to right. The target is placed 40 ± 10 cm upstream of the nominal LHCb collision point, and is adjacent to the RF foils which separate the VELO sensors from the LHC primary vacuum. The lower sketch illustrates the cell in its open position, with the two halves retracted from the beam line. Electrical continuity with the beam pipe is ensured by the flexible structure of the wake field suppressor, which has been redesigned. The indicated lenghts are in mm.

- a metal microstrip target, facilitating a physics program similar to the one discussed here, with a large variety of nuclear targets [20].

The physics possibilities offered by such devices are not covered by the present document.

3 Status of the current fixed-target program

After two short pilot runs on a neon target performed during 2012 (pNe) and 2013 (PbNe), a physics program with SMOG has been carried out during LHC Run 2. Figure 4 summarizes the available data samples, whose size is expressed in terms of delivered protons (or lead ions) on target. After collecting small amounts of data with the 3 possible gas species in 2015, the 2016 runs were dedicated to the study of proton-helium collisions, mostly motivated by the antiproton production measurement discussed in Section 6.1. To avoid background from pp collisions, fixed-target events were recorded when a bunch in beam1, pointing toward the LHCb detector from the interaction point, crosses the nominal interaction region without a corresponding colliding bunch in the other beam. Most of these samples were collected during special runs at low beam intensity (Van der Meer scans, LHC MD periods), without interfering with the standard pp data taking, and are therefore limited in integrated luminosity. However, during pp data taking at $\sqrt{s} = 5$ TeV at the end of 2017, the SMOG device was operated continuously, and the largest fixed-target sample, pNe collisions at $\sqrt{s_{\rm NN}} = 69$ GeV, was collected concurrently with the pp data taking. The corresponding integrated luminosity is of order 100 nb^{-1}. The acquisition of this data sample was mostly motivated by the charm production studies discussed in Section 5.1.

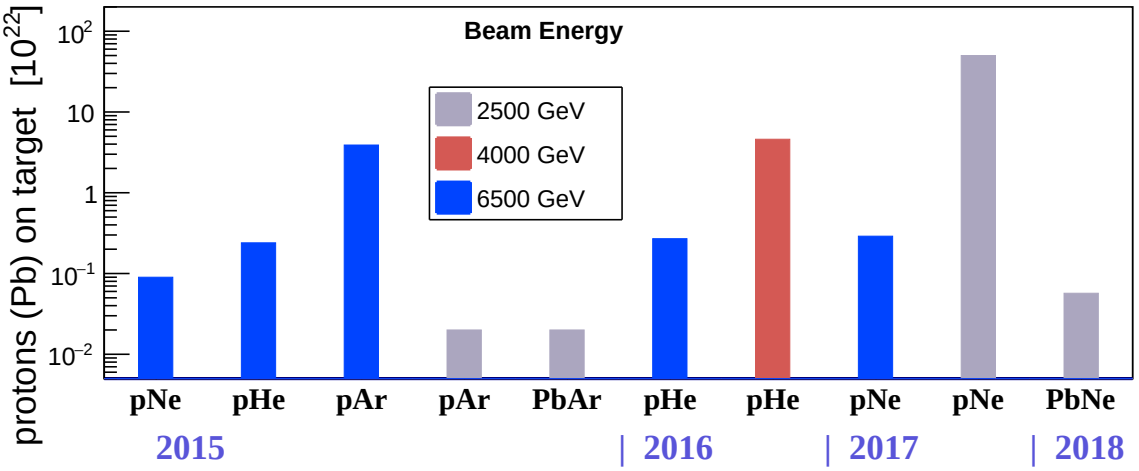

Figure 4: Summary of collected SMOG physics samples. The data size is given in terms of delivered protons (ions) on target (POT). For a nominal SMOG pressure of 2×10^{-7} mbar, 10^{22} POT correspond to an integrated luminosity of about 5 nb^{-1} per meter of gas, though the actual target pressure and the data taking efficiency vary among samples.

The first sample of heavy ion collisions in fixed-target configuration was collected in 2015 during part of the PbPb run, using argon as target gas. A larger sample has been collected using SMOG with a neon target during most of the 2018 PbPb run, allowing for a direct comparison of pNe and PbNe collisions at the same energy.

3.1 Luminosity determination

Measurements of absolute cross-sections require knowledge of the gas target density. As already mentioned, the VELO vacuum vessel is currently not equipped with precisely calibrated pressure gauges. A normalization channel with well known cross-section is provided by elastic proton-electron scattering and was used to determine the integrated luminosity for the first LHCb fixed-target results [21,22]. In this process, only the electron is visible in the detector, as the impinging proton remains inside the beam pipe. Electrons scattered with a polar angle between 10 mrad (the inner detector acceptance) and 22 mrad have a momentum between 10 and 2 GeV, and can be reconstructed in the LHCb spectrometer and identified as electrons in the electromagnetic calorimeter. A multivariate analysis was used to isolate these events from the hadronic background, relying on the specific kinematic properties of the electrons and vetoing additional activity in the detector through a set of multiplicity variables.

The background can be modeled and subtracted using events where the candidate scattered electron track is positively charged, since background is expected to be charge symmetric to a good approximation. The subtraction procedure is illustrated in Fig. 5. The systematic uncertainty on this method was estimated to be 6.0% and is dominated by the uncertainty on the electron reconstruction efficiency [21].

One of the foreseen improvements provided by SMOG2 will be a better control of the target density. Since the beam intensity is also known to better than 1%, the luminosity will be determined with much improved accuracy. It will still be possible to use the scattered electron method as a crosscheck.

3.2 Gas target purity

Residual gas in the LHC machine, whose pressure is typically of order one per cent of the SMOG target pressure and whose composition is unknown, constitutes a possible limitation to the accuracy of beam-gas measurements, notably for light targets. In the absence of beam, the residual gas can be studied with a rest gas analyser. Results indicate that the static residual gas is mostly composed of hydrogen. Additional contamination due to outgassing from the beam pipe material can be induced by the beam and thus depends on the beam intensity and configuration. The composition of this dynamic background could also differ from the static one.

The total residual gas background can be directly measured in special runs, referred to as SMOG vacuum runs in the following, where the same vacuum pumping configuration of the SMOG physics runs is used, but no gas injected. Since at these low pressures molecular flow can be assumed, the beam-gas collision rate due to the residual gas observed during these runs is identical to the one during runs with injected gas and identical beam setup. From 2016 onward, SMOG vacuum runs were always part of fixed-target data taking. Moreover, several SMOG vacuum runs were acquired during the 2017 pp data-taking to directly measure the level of vacuum with high beam intensity.

In the 2016 pHe runs, where the beam intensity was limited to $< 2 \times 10^{13}$ protons, the rate of beam-gas collisions due to background was found to be lower than 1% of the total rate [21]. The average primary track multiplicity was found to be lower in collisions with the residual gas than in collisions with the helium target, confirming that the residual gas is mainly composed of hydrogen. In the SMOG vacuum runs performed with beams

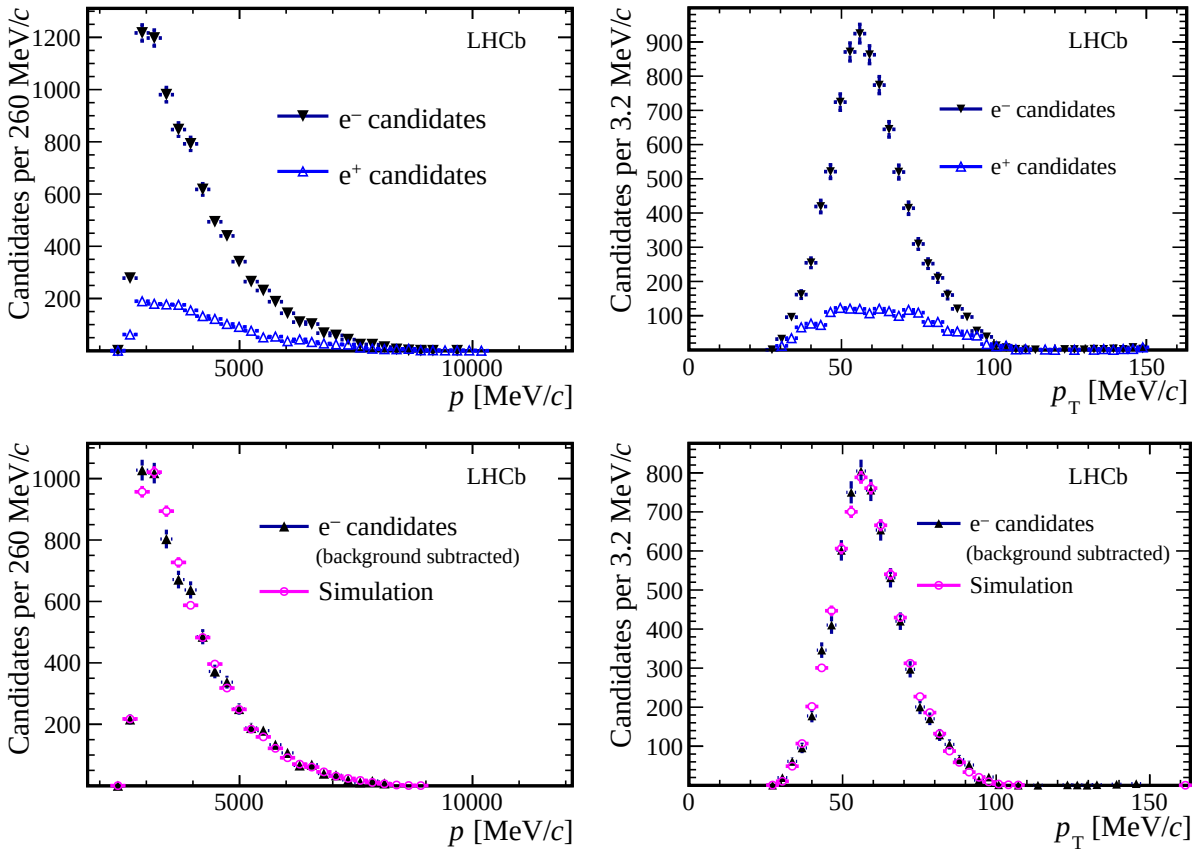

Figure 5: Distributions of (left) momentum and (right) transverse momentum for (top) single electron and single positron candidates, and (bottom) background-subtracted electron candidates, compared with the distributions for the simulated pe^- signal, which are normalized to the data yield. The plots are obtained from the pHe sample at 110 GeV [21]. The single positron candidates are used to model the background.

of nominal intensity, i.e. $1 - 2 \times 10^{14}$ protons, the rate of collisions, normalized to the beam intensity, was found to be larger by up to a factor 10 with respect to the 2016 pHe runs, revealing a dominant contribution from beam-induced residual gas. In this case, the average primary track multiplicity was found to be larger than that in the helium runs, indicating the presence of heavier contaminants.

The effect was also confirmed by the readings of the two Penning gauges located in the VELO area, indicating a large increase of the pressure at beam injection, and a decay corresponding to the decrease of beam intensity, as illustrated in Figure 6. During the 2017 pNe run with 2.5 TeV beams of high intensity, SMOG vacuum runs were performed both at the beginning and at the end of some fills, to be able to interpolate the average background yield. Owing to the heavier target (Ne instead of He), the effect was still limited to a few % level.

The target pressure increase foreseen with SMOG2 is expected to make this background negligible in the future.

Figure 6: Time evolution of the gas pressure of the beam vacuum in the VELO area, measured by two Penning gauges (green and brown lines) during four LHC fills at nominal beam intensity in 2017. The intensity of the LHC beams is shown by the red (beam1) and blue (beam2) lines. The red crosses show, on arbitrary scale, the rate of beam-gas collisions, normalized to beam1 intensity, measured in three SMOG vacuum runs acquired during these fills. Note that the calibration scale of the gauges has large uncertainty, but the relative changes are significant, and in reasonable agreement with the beam-gas rate measurements.

4 Projected integrated luminosities with SMOG2

The large increase in target gas pressure achievable with SMOG2 opens very interesting possibilities for physics channels which are presently limited by the integrated luminosities available with SMOG, like Drell-Yan production of lepton pairs or b-hadron production. Given the novelty of this program and the fact that the main focus of the LHCb physics program remains heavy flavour physics with pp collisions, it is difficult to predict the integrated luminosities that could be collected during Run 3 before acquiring some experience with data-taking and better defining the operational constraints.

The first requirement for fixed-target data-taking is minimal interference with the core LHCb program. During Run 3, the LHCb upgraded detector will be operated in pp collisions at an instantaneous luminosity of $2 \times 10^{33}\text{cm}^{-2}\text{s}^{-1}$, corresponding to an average of 7.6 collisions per beam crossing (5.2 of which are visible in the detector). In these high-pileup conditions, the simultaneous presence of beam-gas collisions with a relative contribution to the detector occupancy of up to a few % is not expected to affect the detector performance. As an example, using a neon target with an average pressure in the storage cell of 2×10^{-5} mbar, 100 times larger than with SMOG, the corresponding luminosity would be $3 \times 10^{31}\text{cm}^{-2}\text{s}^{-1}$, giving an average of 0.4 collisions per bunch (0.3 visible in the detector). Moreover, the SMOG2 geometry avoids a significant background from beam-gas collision vertices in the luminous pp collision region and downstream of it (where beam-gas collisions could be a background to searches for long-lived exotic particles). This opens the possibility of acquiring fixed-target collisions concurrently with pp data taking for a significant fraction of the beam time.

On the other hand, the simultaneous recording of fixed-target and beam-beam inter-

Table 1: Possible scenario for the integrated luminosities to be collected with SMOG2 using different gas targets during the 3 years of Run 3 data taking. For each configuration, the average target pressure is chosen to have less than 0.4 inelastic beam-gas collisions per proton bunch, i.e. below 5% of the expected rate of pp collisions per bunch crossing. The corresponding target areal density ρ_S, the instantaneous luminosity and rate of inelastic beam-gas collisions are given, as well as the expected integrated luminosities for a possible sharing of beam time driven by the physics motivations discussed in the following sections. These numbers assume concurrent beam-gas and beam-beam data-taking with proton beams for one third of the beam time, the exploitation of all available beam bunches for fixed-target physics, and beam intensities of 2.6×10^{14} protons or 2.2×10^{11} lead ions.

System	$\sqrt{s_{\rm NN}}$ (GeV)	$<$ pressure$>$ (10^{-5} mbar)	ρ_S (cm^{-2})	$\mathcal{L}$ (cm^{-2}s^{-1})	Rate (MHz)	Time (s)	$\int \mathcal{L}$ (pb^{-1})
pH$_2$	115	4.0	2.0×10^{13}	6×10^{31}	4.6	2.5×10^{6}	150
pD$_2$	115	2.0	1.0×10^{13}	3×10^{31}	4.3	0.3×10^{6}	9
pAr	115	1.2	0.6×10^{13}	1.8×10^{31}	11	2.5×10^{6}	45
pKr	115	0.8	0.4×10^{13}	1.2×10^{31}	12	2.5×10^{6}	30
pXe	115	0.6	0.3×10^{13}	0.9×10^{31}	12	2.5×10^{6}	22
pHe	115	2.0	1.0×10^{13}	3×10^{31}	3.5	3.3×10^{3}	0.1
pNe	115	2.0	1.0×10^{13}	3×10^{31}	12	3.3×10^{3}	0.1
pN$_2$	115	1.0	0.5×10^{13}	1.5×10^{31}	9.0	3.3×10^{3}	0.1
pO$_2$	115	1.0	0.5×10^{13}	1.5×10^{31}	10	3.3×10^{3}	0.1
PbAr	72	8.0	4.0×10^{13}	1×10^{29}	0.3	6×10^{5}	0.060
PbH$_2$	72	8.0	4.0×10^{13}	1×10^{29}	0.2	1×10^{5}	0.010
pAr	72	1.2	0.6×10^{13}	1.8×10^{31}	11	3×10^{5}	5

actions poses challenging requirements for the online selection system, which could be overcome by limiting the fixed-target data-taking only to beam bunches not colliding in LHCb (about 10% of the total). Also in view of possible limitations from the LHC beam vacuum, the data-taking strategy used for SMOG could be adopted, with fixed-target physics performed only during short dedicated runs where the gas density could be increased beyond the quoted values.

In the following sections, the evaluation of the physics potential will be based on the optimistic yet still realistic scenario shown in Table 1, which assumes to record fixed-target physics data concurrently with pp operations for a sizeable (1/3) fraction of the beam time, exploiting all available beam bunches. A more conservative scenario, corresponding to dedicated data-taking or concurrent data-taking using only non-colliding bunches, is obtained by reducing the integrated luminosities mentioned in the table by a factor 10.

The sharing of the beam time assumed in the table is driven by the physics motivations discussed in more detail in the following sections. The use of a hydrogen target will provide a pp reference to all the studies of nuclear effects, and will open the possibility to determine unambiguously nucleon PDFs in the large-x region, shedding light on the possible intrinsic heavy quark content of the nucleons. The use of a deuterium target will allow for the study of isospin violations in the observed channels. For the study of nuclear effects with proton beams, it is envisaged to collect similar statistics for heavy flavour

production with hydrogen, the heaviest possible target (probably Xe), and at least one intermediate nuclear size among Ne, Ar and Kr.

During the PbPb runs foreseen in Run 3, it will be possible to acquire fixed-target collisions with lead beams. The upgraded detector should allow to reconstruct the most central collisions with a target like argon, while the centrality reach for heavier systems like PbXe still has to be determined. Reference pA samples at the same energy scale of 72 GeV can be obtained by using both a hydrogen target with lead beams, and an argon target during the foreseen reference pp run at 5.5 TeV.

The use of gas types not employed so far (H_2, D_2, O_2, N_2, Kr, Xe) and their impact on the machine is being addressed in the PBC Fixed targets working group, in cooperation with the LHC machine experts [23]. The amount of injected getterable gases may be limited by the integrity of the NEG coating in the vicinity of IP8. Molecular flow simulations, surface coverage estimations and, for H_2 and D_2, embrittlement limit estimations are still to be performed. The same applies to the heavy (non-getterable) noble gases Kr and Xe which will be cryosorbed at the warm-to-cold transitions of the triplet quadrupoles and cause an increase of the local secondary electron yield. The impact on the LHC, limitations in quantities injected and possible countermeasures must be carefully explored. These detailed studies could reduce the numbers assumed here for the total amount of injected gas.

5 Heavy ion physics

5.1 Heavy quark and Drell-Yan production in the nuclear medium

Relativistic heavy ion collisions give access to the high-density and high-temperature regime of QCD, where the production of heavy quarks is well suited to studies of the phase transition between ordinary hadronic matter and the Quark-Gluon Plasma (QGP), where partons are asymptotically free from color confinement. Since their masses are significantly higher than the QGP critical temperature ($\sim$156 MeV), heavy quarks are only produced in the early stages of the interaction. Therefore, the later QGP phase should not modify the overall heavy quark yields, while the deconfinement is expected to significantly affect the formation of hidden heavy-flavour bound states, an effect that is considered as one of the key signatures for QGP formation [24]. As the screening (or dissociation) temperature depends on the radius of the $q\overline{q}$ bound state, a larger suppression is expected for excited states, an effect known as sequential suppression [25].

However, quarkonium production in nuclear collisions is affected by several other effects. Parton shadowing and anti-shadowing [26] or saturation effects [27] modify the probability of heavy quark production in the nuclei. Interactions of the initial and final partons with the surrounding nuclear matter is expected to cause energy loss [28], notably at large rapidity. Interactions of the final state with cold nuclear matter [29, 30] or with comoving particles [31, 32] can lead to the break-up of the $c\overline{c}$ pair. On the other hand, notably when increasing the energy to the TeV scale, charmonia secondary production via statistical recombination [33] can occur.

To investigate and disentangle these physical processes, measurements of heavy quark production covering a wide range of collision systems, collision energies and kinematic

acceptances are needed. In particular, the study of charmonium production in proton-induced reactions on various nuclear targets, where QGP is not expected to be formed, is needed to establish a robust baseline so that the QGP-induced suppression patterns observed in heavy-ion collisions may be interpreted correctly. This is also crucial to understand the physics mechanisms underlying charmonium production [34].

The LHCb collaboration demonstrated that its detector can perform unique measurements of heavy hadron production in proton-lead collisions at forward rapidity [35–41]. The fixed-target configuration provides the unique possibility to perform these studies at $\sqrt{s_{\rm NN}} \sim 40-115$ GeV, filling the gap between experiments at the SPS ($\sqrt{s_{\rm NN}} \sim 10-30$ GeV) and the highest energies reached at RHIC ($\sqrt{s_{\rm NN}} \sim 200$ GeV) and LHC ($\sqrt{s_{\rm NN}} \sim 5-8$ TeV). Combining different LHC beams with different target gas species, a wide range of collision systems, from pp to PbXe, can be investigated.

The other clear advantage of the fixed-target configuration is the possibility to study parton PDFs in the high-x region, where they are affected by relevant nuclear effects: the enhancement with respect to free nucleons around $x \sim 0.1$ known as antishadowing, and the EMC suppression at larger x values, whose interpretation is still debated. In particular, the PDFs for gluons and sea quarks and the flavour-dependence of the nuclear effects are still poorly constrained [42]. Measurements from LHCb in fixed-target pp collisions could be conclusive on establishing the amount of intrinsic charm inside the nucleon [43, 44]. The confirmation of this prediction from QCD would be of fundamental importance by itself, and would have consequences for collider physics, as some high-Q^2 processes can be affected [45–48], and for cosmic ray physics, as discussed in Section 6.2.

The feasibility of these studies with LHCb has been demonstrated using two of the first collected fixed-target samples, namely pAr collisions at $\sqrt{s_{\rm NN}} = 110$ GeV and pHe collisions at $\sqrt{s_{\rm NN}} = 87$ GeV [22]. Samples of order 10^2 J/ψ candidates and 10^3 D^0 candidates were reconstructed, with excellent mass resolution and purity, from both samples, which correspond to less than 10 nb^{-1} of integrated luminosity. Despite the limited statistics, these recent results provide the first determination of the $c\bar{c}$ cross-section at this energy scale (see Figure 7), and the rapidity dependence shown in Figure 8, notably with the helium target, is already expected to provide significant constraints for the amount of intrinsic charm in the target nucleons.

The largest SMOG sample of pNe collisions at 69 GeV will allow to increase the charm statistics by more than one order of magnitude, allowing for a first study of charm baryon production. The latter is particularly interesting since production of Λ_c^+ baryons could be boosted at large x by the contribution from coalescence of intrinsic charm quarks. Moreover, the Λ_c^+ over D^0 ratio is expected to be enhanced by the formation of QGP, as indicated by the recent results at RHIC [56] and the LHC [57], though unexpectedly large values for the Λ_c^+ fragmentation fraction have also been observed in pp and pPb collisions at mid-rapidities by ALICE [58] and in pPb collisions at forward rapidities by LHCb [40].

The potential of the samples achievable with SMOG2 during Run 3 is summarized in Table 2, where rough estimates for the expected yields of reconstructed events for some of the most interesting channels are given for a sample of 45 pb^{-1} of pAr collisions and compared with the achievable yields with current SMOG samples. Production rates of charmed particles are extrapolated from the ones measured in pHe collisions, assuming absorption by the nuclear target leading to a decrease by a factor 0.75 (0.6) in pNe and 0.5 (0.4) in pAr for J/ψ ($\psi(2S)$) with respect to pHe. The smaller systematic uncertainty on the J/ψ production cross-section determination with SMOG2 is expected

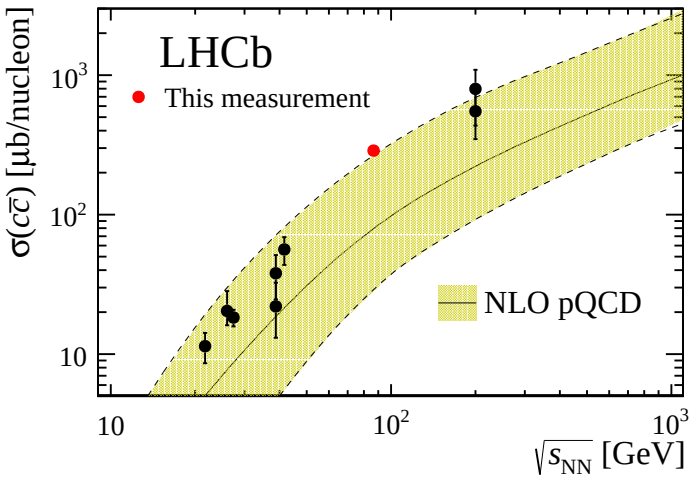

Figure 7: Results for the $c\bar{c}$ cross-section measurements as a function of the centre-of-mass energy. Previous experimental data, shown by the black points, are taken from Ref. [49]; the yellow band corresponds to NLO pQCD calculations [50]; the red point corresponds to the LHCb result obtained from the pHe fixed-target data [22].

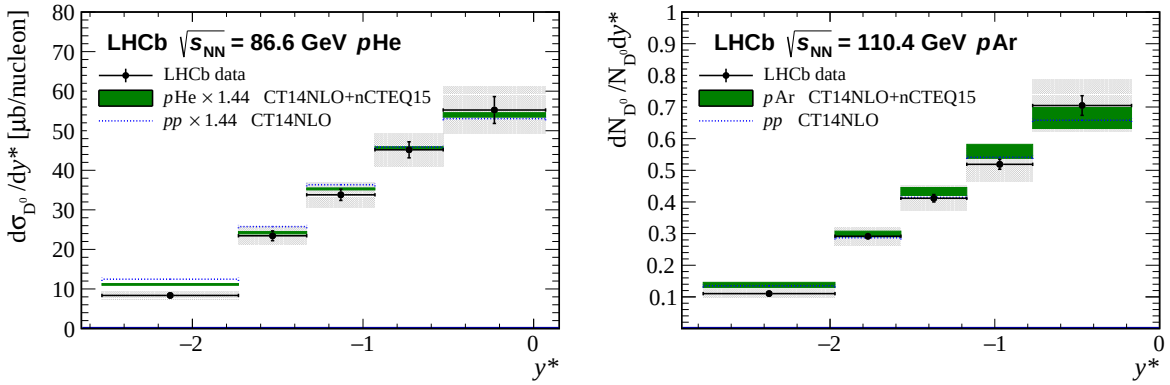

Figure 8: Differential D^0 production cross-sections for (left) pHe collisions at 110 GeV and differential D^0 yields for (right) pAr collisions at 87 GeV, as a function of centre-of-mass rapidity y^*. The data points mark the bin centres. The quadratic sum of statistical and uncorrelated systematic uncertainties is indicated by the vertical black lines. The correlated systematic uncertainties are indicated by the grey open boxes. Results have been compared with HELAC-ONIA predictions [51–53], for pp (CT14NLO PDF set [54]) and pHe, pAr (CT14NLO+nCTEQ15 PDF [55] sets) collisions. These predictions underestimate the measured total cross-section in pHe by a factor 1.44, which has been used to rescale the HELAC-ONIA predictions.

from the reduction of the dominant uncertainty for SMOG data, due to the luminosity determination. Figure 9 illustrates the expected statistical accuracy for the determination of the J/ψ $p_{\rm T}$ spectrum. The integrated luminosities assumed in Table 1 would allow accurate measurements of $\psi(2S)$ and χ_c production in different systems, providing novel inputs to the interpretation of sequential charmonia suppression.

Production of b hadrons would be also within reach, with about 7k reconstructed $\Upsilon(1S) \to \mu^+\mu^-$ decays expected from 45 pb^{-1} of pAr collisions. This estimate is obtained assuming the same selection and reconstruction efficiency as for the pp analysis

Table 2: Expected yields of reconstructed events for selected processes using fixed-target data samples acquired with SMOG during the LHC Run 2, and possible with SMOG2 during Run 3 (using as an example the pAr sample according to the scenario in Table 1).

	SMOG published result pHe@87 GeV	SMOG largest sample pNe@69 GeV	SMOG2 example pAr@115 GeV
Integrated luminosity	7.6 nb^{-1}	$\sim$ 100 nb^{-1}	$\sim$ 45 pb^{-1}
syst. error on J/ψ x-sec.	7%	6 - 7%	2 - 3 %
J/ψ yield	400	15k	15M
D^0 yield	2000	100k	150M
Λ_c^+ yield	20	1k	1.5M
$\psi(2S)$ yield	negl.	150	150k
$\Upsilon(1S)$ yield	negl.	4	7k
Low-mass Drell-Yan yield	negl.	5	9k

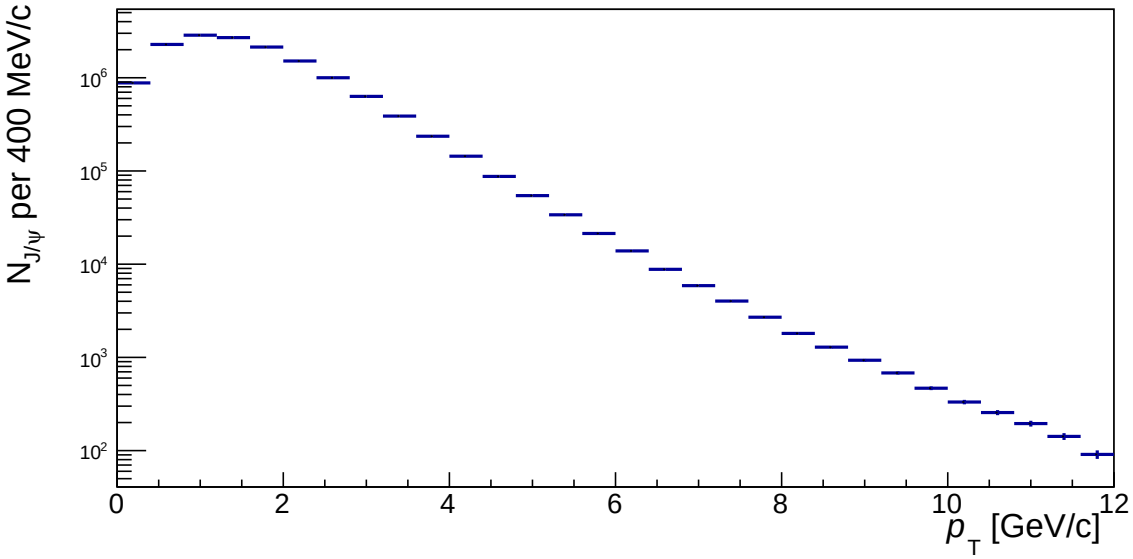

Figure 9: Expected reconstructed $p_{\rm T}$ spectrum for J/ψ in pAr collisions, using 45 pb^{-1} of SMOG2 data. Error bars, barely visible, represent the statistical uncertainties.

at 7 TeV [59], scaling the pp cross-section by a factor 0.008 calculated by means of PYTHIA8 [60], and assuming a nuclear absorption factor of 0.6.

Production of Drell-Yan muon pairs can be measured in LHCb above the J/ψ mass, as demonstrated in pp collisions [61], and gives access to the sea quark PDFs. The fixed-target LHCb configuration allows a substantial increase of the kinematic reach with respect to past fixed-target experiments, as shown in Figure 10. As a benchmark, we consider the production cross-section for di-muon masses between 5 and 9 GeV/c^2 in pAr collisions, requiring muons to have momentum above 10 GeV and $p_{\rm T}$ above 3 GeV. The cross-section has been measured to be about 300 pb for pp collisions at 7 TeV in Ref. [61]. Assuming the same experimental efficiency and scaling the pp production cross-section by a factor

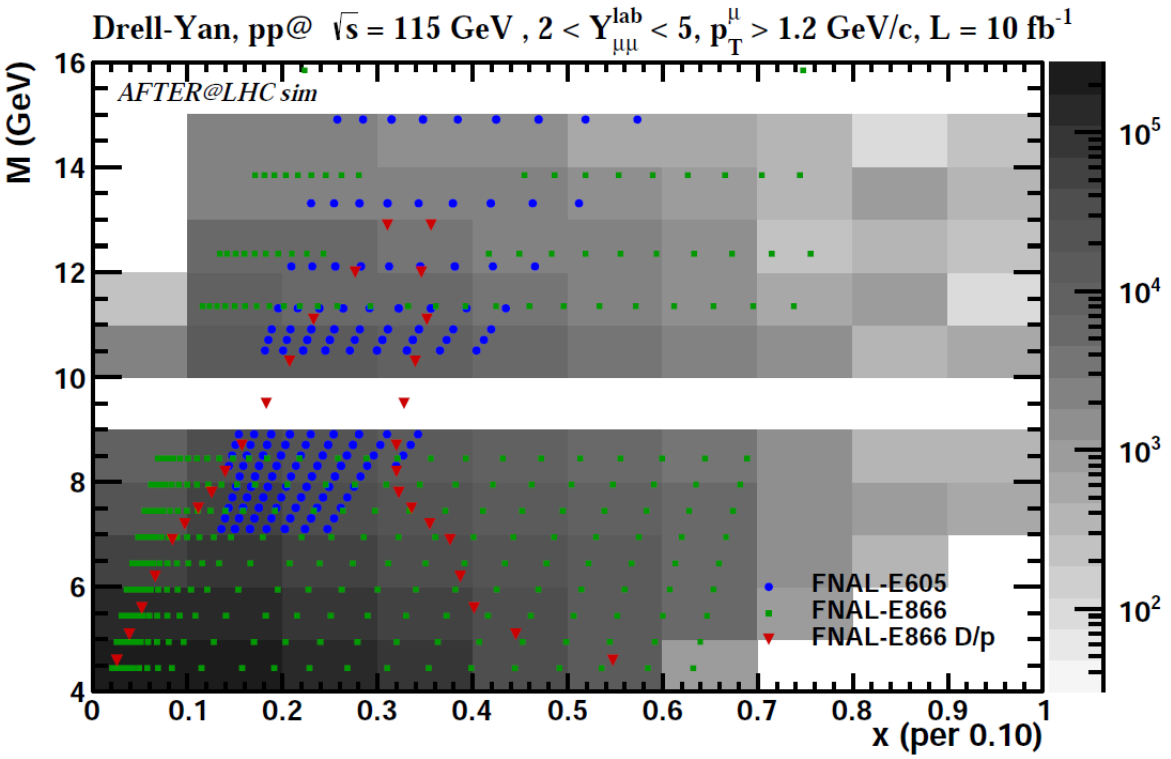

Figure 10: Comparison of the kinematic reach for DY muon-pair production between fixed-target LHCb (gray histogram) and existing data used in current global PDF fits (coloured points). The histogram represents the number of events for 10 fb^{-1} of pp collisions. Estimation performed by the AFTER collaboration [3].

0.053 according to the PYTHIA8 prediction, only about 5 events should be found in the largest SMOG sample. With the SMOG2 setup, a sample of about 9k reconstructed events can be obtained from 45 pb^{-1} of pAr collisions, opening the possibility for a precision measurement.

A comprehensive analysis of the impact on nuclear PDFs achievable with fixed-target measurements at the LHC has been performed by the AFTER collaboration [2, 3].

5.2 Flow and fluctuations

The hydrodynamic description of the QCD medium produced in heavy-ion collisions can be tested in fixed-target data down to the energy of $\sqrt{s_{\rm NN}} \sim 70$ GeV through measurements of flow observables and correlations at central rapidities for a variety of collision systems. Flow measurements can exploit the excellent particle identification capabilities for charged pions, kaons and protons as well as for neutral particles ϕ, $K^0_{\rm S}$ and Λ. These studies can shed light on the extension of the hydrodynamic description [62, 63], which is very successful at the highest RHIC energies and, with an appropriate treatment of the baryon density [64] and a fully three-dimensional description of the initial state [65], in the lower range of the LHC energies. A comprehensive fluid-dynamical description of lower-energy collisions with finite baryon density with an appropriate dynamical treatment will be important in the search for the critical point in the QCD phase diagram [66, 67]. The

LHCb fixed-target programme, still at comparatively high beam energies but with a considerable pseudorapidity coverage, three units from mid- towards the beam rapidity, presents a very good testbed for fluid dynamical descriptions at finite baryon number and models of baryon stopping and may allow for measurements of material properties such as shear and bulk viscosity. In addition, the extension of the fluid dynamical paradigm towards smaller collision systems as an explanation of the experimental findings in proton(deuteron)-nucleus and pp collisions at the LHC [68–72] and at RHIC [73] can be probed with particle identification over a large acceptance and high luminosities at lower beam energies, contributing to the understanding of the observed phenomena with an additional control parameter, the collision energy.

5.3 Ultra-peripheral collisions

Photon-induced processes, which can be studied in ultraperipheral collisions (UPC) among nuclei, when the impact parameter is large compared to the nuclear sizes, provide a rich testing ground for QCD. The LHC provided a novel kinematic regime, down to very low values of x where the gluon PDF can be probed in a regime where non-linear effects inherent to non-perturbative QCD may become evident. LHCb contributed to this physics by measuring exclusive production of quarkonia [74, 75] and bottomonia [76] states from pp collisions in the forward region, where the gluon density can be probed down to $x \sim 5 \times 10^{-6}$ at the scale of a few GeV. As the photon flux is proportional to the squared atomic number of the colliding nuclei, interesting measurements for UPC physics are possible also in the smaller samples of pPb collisions and PbPb collisions, where coherent J/ψ photoproduction has indeed been observed [77].

The fixed-target configuration provides a complementary kinematical regime for these studies, with lower values for the γ-hadron or γ-γ center-of-mass energy. An intriguing possibility would be the observation of η_c photoproduction in the PbAr sample, where the cross-section is estimated to be of order 1 nb [78]. This would constitute a confirmation for the existence of the odderon, since the η_c state cannot be produced in the γ-pomeron process and would be under threshold for the γ-γ process in fixed-target PbA collisions, provided that the background from radiative J/ψ decay can be properly subtracted [79]. Large samples of exclusively produced ρ^0 and ω are expected [80], and the SMOG2 luminosities are expected to allow the observation of photoproduced charmonia and bottomonia states in the fixed-target configuration.

These studies are not expected to be possible for most of the Run 2 fixed-target samples, given the low efficiency of the online selection used during SMOG runs. However, the experience gained by the collaboration with UPC physics lead to the implementation of dedicated selections during the last fixed-target data-taking with PbNe collisions, and these studies will be developed for future running.

5.4 Polarization in baryon production

At 100 GeV centre-of-mass energy, Λ_c^+ baryons are expected to be produced with a substantial polarization. This allows the possibility to measure the magnetic and electric dipole moments (MDM/EDM) of heavy baryons by observing the spin precession induced by an effective strong magnetic field inside bent crystals. It was recently proposed to perform this experiment with Λ_c^+ baryons produced in a solid fixed target close to the

LHCb vertex detector and channeled through bent crystals [14–17]. The measurement of the Λ_c^+ polarization in fixed-target collisions is therefore not only interesting as a QCD testbench, but also input to evaluate the sensitivity of a possible future MDM/EDM measurement.

In peripheral heavy ion collisions, in systems like PbAr or PbXe, a global mean polarization of the produced particles, directed along the direction of the angular momentum of the nuclear medium produced by the collision, is expected as a quantum manifestation of the strong vorticity of the a QGP formed in such interactions. The effect has been recently discovered at RHIC by the STAR collaboration [81], who observed a mean polarization of the Λ baryons by a few per cent, consistent with hydrodynamic predictions [82]. While the effect is expected to be vanishingly small in beam-beam collisions at the LHC, fixed-target collisions provide an energy scale where the effect could be detectable, and thus the possibility for measurements complementary to results from RHIC in terms of collisions systems and kinematic configuration.

5.5 Worldwide Context

LHCb is presently the only experiment using the LHC beams for a fixed-target physics program. The signal yields attainable with this program for heavy hadron production, and other rare processes like Drell Yan and photoproduction in UPC, are unrivaled for the covered energy range of $\sqrt{s_{\rm NN}} \sim$ 40-100 GeV. Experiments at RHIC cover a similar energy scale only in beam-beam collisions, with smaller integrated luminosities and without coverage of the large x region. The proposed fixed-target program of ALICE is expected to provide measurements with different and complementary angular acceptance and detector capabilities, and will be possible on a longer timescale ($>\sim$2026).

6 Hadronic particle production and cosmic ray physics

Understanding the bulk of particle production in high-energy hadronic collisions is an open challenge for the theory of strong interactions, since the contribution of non-perturbative QCD effects in the soft or high-density regions becomes dominant, with the consequence that perturbative QCD cannot be used to predict total inelastic cross-sections. Beside the theoretical interest, knowledge of the multiplicity and spectra of particles produced in hadronic collisions, notably at large x, is important to model the underlying event for hadron collider physics, and crucial to understand production of secondary particles in the propagation of cosmic rays through the interstellar gas (ISG) and the atmosphere. Phenomenological models combine the rigorous description of the hard parton-parton scattering provided by perturbative QCD with an effective description of the soft component, based on general principles of quantum field theories such as unitarity and analyticity. These models require tuning to experimental data, and the kinematic regime offered by LHCb in its fixed-target configuration is unique. Production measurements of exclusive states which are of particular interest to cosmic ray physics are possible, owing to the possibility to use different gas targets, i.e. different propagation media, and the excellent particle identification capabilities of the detector.

6.1 Cosmic ray collisions in the interstellar medium

In recent years, the space-based cosmic-ray detectors PAMELA [83] and AMS-02 [84] have dramatically improved our knowledge of the cosmic-ray composition for energies up to 500 GeV. The antimatter content in cosmic rays is a sensitive indirect probe for exotic sources of antimatter production, like dark matter annihilation. Current results for the production ratio of antiprotons over protons, shown in Figure 11, indicate a slight tension with predictions of the expected $\overline{p}$ fluxes due to known processes, namely secondary production in collisions between primary cosmic rays and the ISG, which is essentially composed of hydrogen (90%) and helium (10%). In the 10 to 100 GeV range of $\overline{p}$ energy, the largest uncertainty on such predictions is due to the limited knowledge of the $\overline{p}$ production cross-sections in the relevant processes. Since these cross-sections can be predicted in phenomenological models only within large ($\sim$ factor 2) uncertainties, computations of the expected $\overline{p}$ flux are based on extrapolations of existing measurements. There are different sources of uncertainty affecting these calculations (see e.g. [85–87]):

- before LHCb, no measurements were performed in pHe collisions, which account for about 40% of the $\overline{p}$ production (cosmic protons on helium gas or cosmic He on hydrogen gas);
- data for $\overline{p}$ production in pp collisions are also sparse; predictions are mostly based on the NA49 [88] and NA61 [89] results at the CERN SPS, limited to $\sqrt{s_{\rm NN}} < 30$ GeV. The accuracy of extrapolations to higher energy scales, which contribute to the fluxes of $\overline{p}$ above 10 GeV, are affected by violations of Feynman scaling. Measurements at higher $\sqrt{s_{\rm NN}}$ are therefore desirable;
- there is poor knowledge about production of anti-hyperons, which are expected to

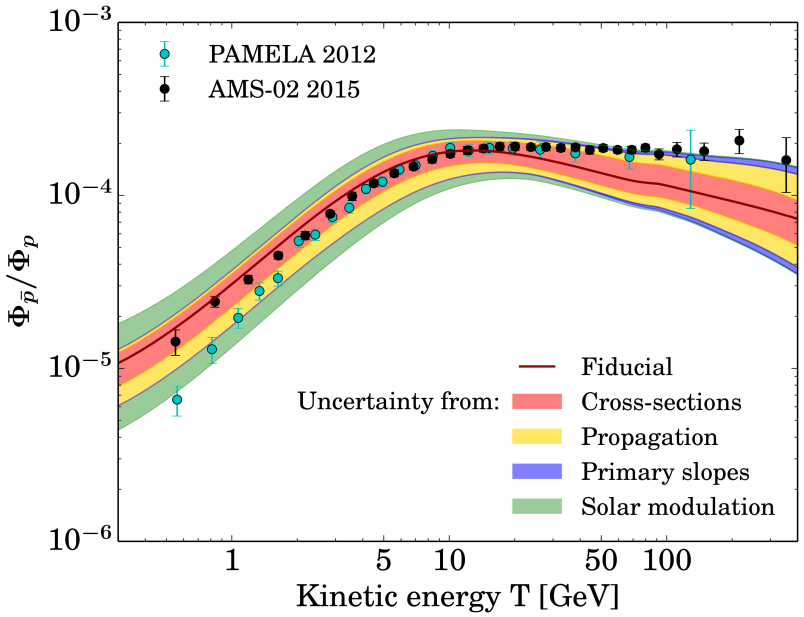

Figure 11: The combined total uncertainty on the predicted secondary $\overline{p}/p$ ratio, superimposed on the older PAMELA data and the new AMS-02 data (from [85]).

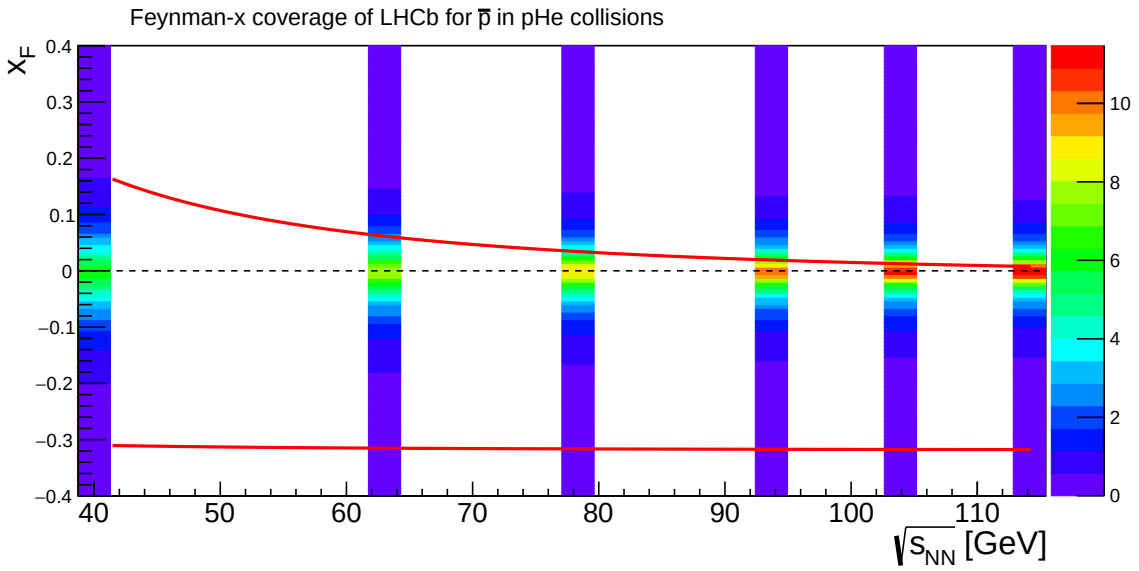

Figure 12: The graph shows the expected Feynman-x, x_F, probability density function for antiprotons with momentum between 12 and 110 GeV, produced in pHe collisions at different c.m. energies, according to the QGSJETII04m model [94]. The two thick lines indicate the minimum and maximum values of Feynman-x accessible to LHCb for antiprotons with p_{T} below 2 GeV.

constitute 20-30% of the total $\overline{p}$ production;

- there are no direct data on antineutron production at the relevant energies. The usual assumption of equal $\overline{p}$ and $\overline{n}$ production is affected by possible isospin violation, which is poorly constrained. Data from the NA49 collaboration showed hints for a sizeable isospin violation when comparing $\overline{p}$ production in pp and dp collisions [90].

With its fixed-target program, LHCb has the potential to address all these sources of uncertainty. Using the pHe SMOG data collected in 2016, the experiment performed the first measurement ever of $\overline{p}$ production in pHe collisions. The first result was released for prompt $\overline{p}$ production at $\sqrt{s_{\mathrm{NN}}} = 110$ GeV [21]. The accessible $\overline{p}$ energy range, 12 to 110 GeV, nicely matches the range of interest for the capabilities of the AMS-02 spectrometer. At $\sqrt{s_{\mathrm{NN}}} = 110$ GeV, the LHCb acceptance covers central and negative rapidities in the c.m. frame ($-0.24 < x_F < 0$), corresponding to 35-42%[1] of the total $\overline{p}$ production in the selected momentum range. LHCb can in principle cover the beam energy range from 0.9 TeV [2] to 7 TeV ($41 < \sqrt{s_{\mathrm{NN}}} < 115$ GeV), so that the deviation from scaling behaviour in the evolution of the cross-section can be observed through the whole range of interest. As shown in Figure 12, at lower energy the detector acceptance also has sensitivity to positive values of Feynman-x. Data with 4 TeV beam energy have been already collected.

Figure 13 shows the accessible $\overline{p}$ kinematic region and the relative accuracy of the first measurement, which is below 10% for most kinematic bins. The study is being extended

[1] the range is obtained from the predictions of the EPOS LHC [91], EPOS 1.99 [92], HIJING [93] and QGSJETII04m [94] models

[2] at the LHC injection energy of 450 GeV the measurement can't be performed since the beam optics forbid LHCb to close the VELO.

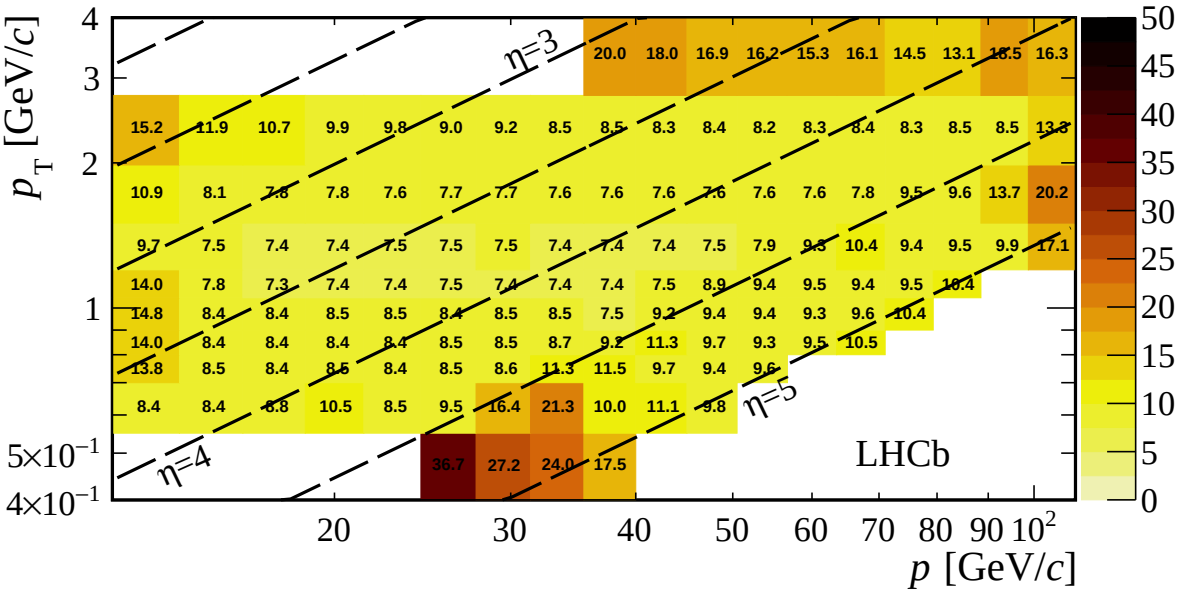

Figure 13: Total relative uncertainty in each kinematic bin for the $\overline{p}$ production cross-section measurement in pHe collisions at $\sqrt{s_{\rm NN}} = 110$ GeV, in per cent [21].

to the production of antiprotons from anti-hyperon decays. As a sizeable fraction of the $\overline{\Lambda}$ and $\overline{\Sigma}$ decays producing detached antiprotons occur within the detector, we expect a measurement of this component with comparable accuracy to the prompt one.

One of the aims of SMOG2 is the possibility to inject hydrogen and deuterium. Repeating the study in pp collisions would provide the opportunity to extend the measurement of $\sigma(pp \to \overline{p}X)$ from SPS energies up to $\sqrt{s_{\rm NN}} = 115$ GeV, and to determine precisely the ratio $\sigma(p\text{He} \to \overline{p}X)/\sigma(pp \to \overline{p}X)$, where many systematic uncertainties cancel. The measurements with a deuterium target would test isospin symmetry in the ratio $\sigma(p\text{D} \to \overline{p}X)/\sigma(pp \to \overline{p}X)$, which can be turned into a constraint on $\sigma(pp \to \overline{n}X)/\sigma(pp \to \overline{p}X)$.

Thanks to the detector PID capabilities, secondary production of other particles in the ISG can be investigated:

- light charged mesons, with π^+ and K^+ production, which would lead to an improved prediction for the secondary positron flux;
- high-energy photons, which are a background to γ astronomy;
- light anti-nuclei ($\overline{d}$,$^3\overline{\text{He}}$,$^4\overline{\text{He}}$): this would be particularly interesting, as observation of these particles in space-borne experiments like AMS-02 and GAPS [95] would be considered as a smoking gun for new physics contributions [96]. However, also these states can be produced in interactions with the ISG through coalescence. The production cross-section has been measured at the LHC by ALICE in pp collisions at $\sqrt{s}$ between 0.9 and 7 TeV [97], but there are still large uncertainties on its dependence on the energy and on the collision system. Unlike the ALICE case, identification of nuclei was not among the physics requirements in the design of the LHCb detector. However, ongoing studies indicate that the RICH detector could provide some identification capability at least for anti-deuterons. Measurements in

fixed-target mode would probe the energy scale that is expected to be most relevant for the production of cosmic anti-nuclei and would benefit from the wide choice of gas targets, including hydrogen and helium.

Most of these measurements can be performed with small samples, of order 1 nb^{-1}, of integrated luminosity, like the ones already collected with the SMOG system (the first pHe antiproton result is based on 0.5 nb^{-1}, and its accuracy is limited by systematic uncertainties). The higher luminosity available in SMOG2 opens the possibility to measure antinuclei production, provided that the related identification capabilities are demonstrated and can be implemented in the online event selection.

6.2 Cosmic ray collisions in the atmosphere

Understanding the composition and energy spectrum of the ultra-high-energy (UHE) component of cosmic radiation is one of the main challenges in astroparticle physics [98]. Properties of cosmic rays with energies above $\sim 10^{14}$ eV can be measured only indirectly through the observation of extensive air showers, whose interpretation is presently limited by the uncertainties in models of hadron production [99, section 11.3] [100]. The LHC data in collision mode for the first time provided access to pp and pPb collisions at an energy scale corresponding to primary cosmic rays of energy $\sim 10^{17}$ eV, above the so-called knee of the cosmic ray spectrum.

Fixed-target interactions at LHCb correspond to a much lower cosmic ray energy, but still unprecedented for fixed-target experiments, up to 7 TeV. However, the longitudinal development of the atmospheric showers largely depends on ion collisions in the peripheral region of the shower. The fixed-target configuration is thus complementary to studies in beam-beam collisions [101]:

- wider choice of collision systems, including light nuclei: interactions in air can be modeled by interpolating the currently available SMOG samples (pHe, pNe and pAr), while nitrogen and oxygen targets could be possible with SMOG2;

- access to production at large $|x_F|$ values, which is relevant for the understanding of the dissipation of the primary particle energy. Note that the backward particles in the c.m. frame which are detectable in LHCb correspond to particles with rapidity up to 7.6 and energies up to the TeV scale in the rest frame of the impinging nucleon. So, using ion beams on a hydrogen target, very forward production in the pA system can be accessed.

The main background for the observation of the astrophysical high-energy neutrino flux, recently established by the IceCube collaboration [102], originates from neutrinos of PeV energy produced in decays of charmed hadrons in UHE atmospheric showers. The prediction of this background is based on extrapolations of the charm production cross-section measured, in particular by LHCb, in beam-beam collisions [103, 104]. However, as shown in Figure 14, a sizeable uncertainty is related to the possible intrisic charm contribution to the charm PDF at large x [105]. As already discussed in Section 5.1, only charm production studies in fixed-target configuration have the potential to draw conclusions on the actual amount of intrinsic charm.

Measuring the production of light hadrons is also important to understand the development of UHE air showers. The lateral density profile of muons in a shower is one

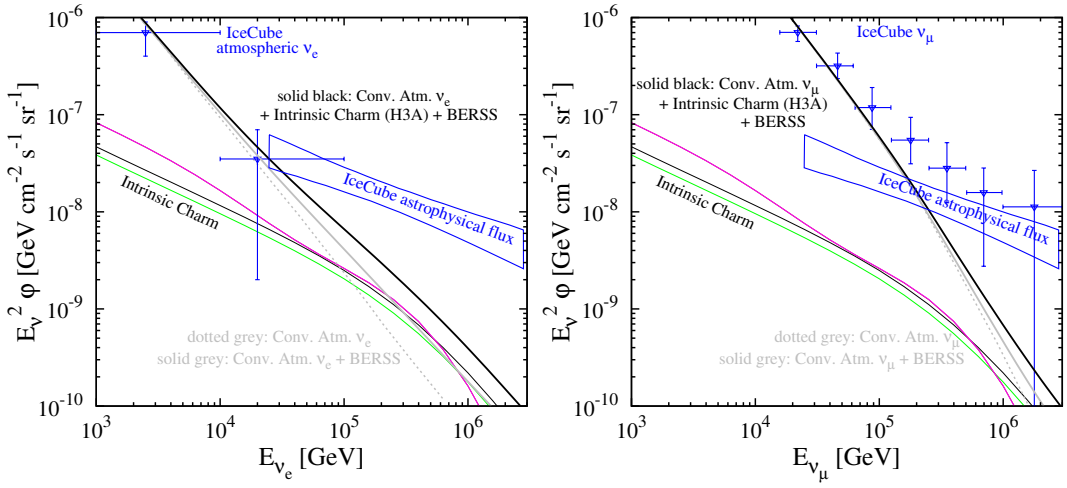

Figure 14: Impact of a possible intrinsic charm contribution to the background for the observation of astrophysical neutrinos at the PeV scale(from [105]). Flux measurements for (left) ν_e and (right) ν_μ neutrinos by the IceCube experiment [106, 107] are compared with predictions for the atmospheric flux with and without intrinsic charm contribution.

of the main observables used by ground-based arrays to infer the composition of cosmic rays. The muon density is very sensitive to the mass number, but the relation depends strongly on the multiplicity and spectra of protons, kaons and pions produced in the shower. Measurements of the muon lateral profile in ultra-high energy air showers in the majority of experiments significantly diverge from model predictions [108]. Addressing this Muon Puzzle requires measurements of hadronic production over a wide energy range with much better accuracy than the current spread among phenomenological models. This is particularly true for baryons, since the uncertainty is larger in that case (see Figure 15), and a sizeable fraction of muons is expected to originate from decays of mesons produced in interactions of protons and neutrons [109]. LHCb can perform this measurement in pA collisions at $\sqrt{s_{\rm NN}} \sim 100$ GeV with an accuracy of a few %, using samples of order 1 nb^{-1} of integrated luminosity. Results with He, Ne and Ar targets are expected from the Run 2 data samples, while the studies could be extended in the future with more gas species, notably nitrogen and oxygen for a direct measurement of particle production for interactions of TeV protons in the atmosphere.

6.3 Worldwide Context

LHCb is presently the only experiment using the LHC beams in fixed-target configuration, and currently, at least until 2026, the only place where the measurements discussed above can be performed at an energy-scale of $\sqrt{s_{\rm NN}} \sim$ 40-100 GeV. The proposed fixed-target program of ALICE is expected to provide measurements with different and complementary angular acceptance and detector capabilities.

The fixed-target program at the SPS accelerator is providing measurements similar to the ones discussed in this Section at a complementary energy range of $\sqrt{s_{\rm NN}} < 30$ GeV. No other $\overline{p}$ production measurements with a helium target have been performed so far, though a proposal at SPS energies has been recently put forward [113].

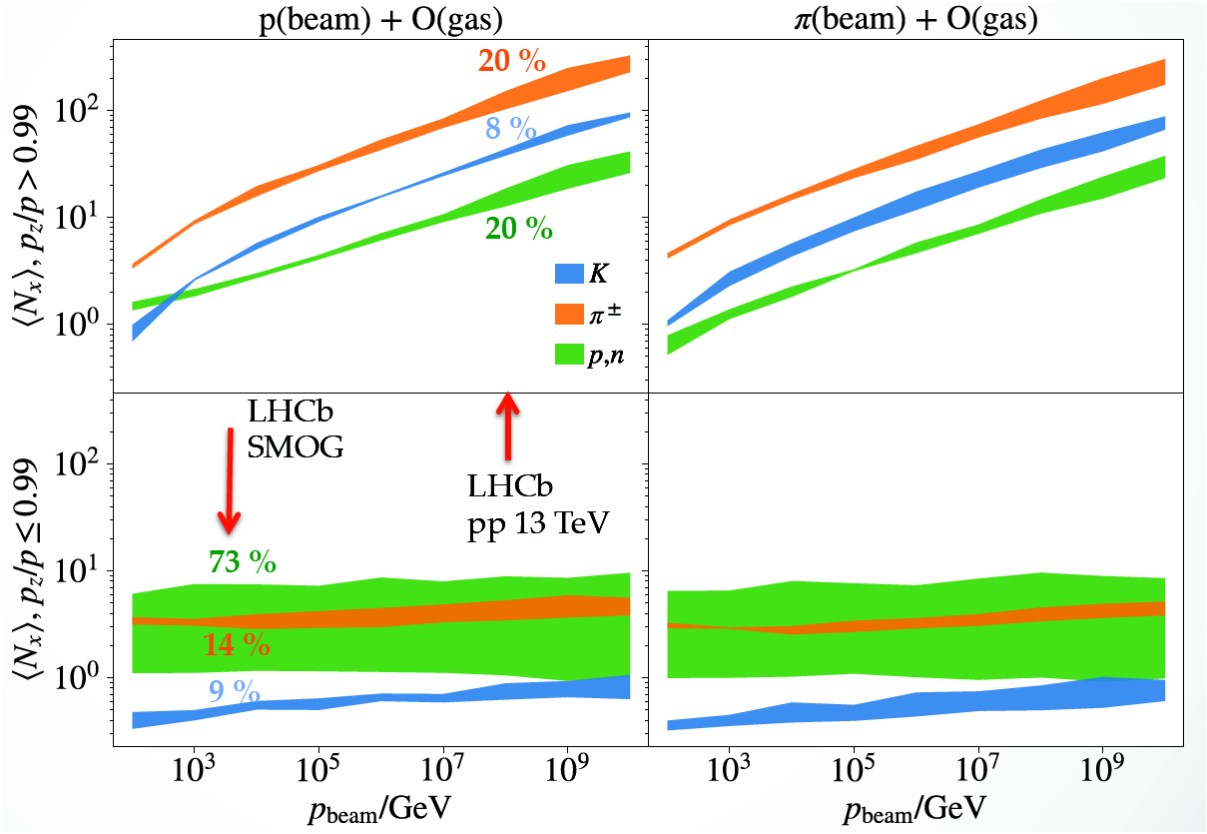

Figure 15: Spread among phenomenological models for the multiplicity of charged pions, charged kaons and protons produced in the (upper plots) forward and (bottom plots) lateral directions, for (left plots) pO and (right plots) πO collisions as a function of the energy of the impinging particle. The spread is calculated from the predictions of the EPOS-LHC [91], QGSJet-II-04 [110] and SIBYLL-2.3 [111] models implemented in the CRMC package [112].

7 Nucleon structure

The nucleon structure is traditionally parametrized in terms of parton distribution functions (PDFs), which, in their simplest (collinear) form, are functions of the longitudinal momentum fraction of quarks and gluons, expressed by the Bjorken-x variable. Although tremendous advances have been made over the past decades in defining the quark and gluon dynamical substructure of the nucleon, the present knowledge of the PDFs still suffers from large uncertainties, especially at very high and very low x [114], leaving open fundamental questions about QCD and confinement. As an example, Fig. 16 shows the situation of the u and d quark PDFs based on some of the latest parameterizations [115]. In many cases, the PDF uncertainties have become the limiting factor in the accuracy of the predictions for LHC measurements. This is particularly critical for the case of precision measurements of SM and BSM observables, where PDFs at high-x constitute an important input for predictions [116, 117].

In this context, SMOG2 offers a unique opportunity to probe quark and gluon PDFs in nucleons and nuclei, especially at high-x and moderately-high Q^2, where the experimental data are still largely missing and unable to constraint the theoretical distributions. Among the processes of interest, Drell-Yan and weak-boson production are particularly suitable

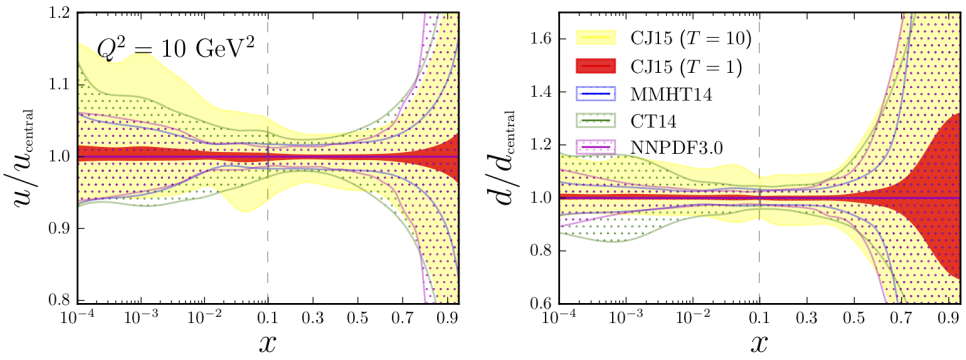

Figure 16: Ratio of PDFs to the CJ15 parameterization central values for various PDF sets [115].

to reduce the uncertainties on the light quark and anti-quark PDFs in a wide kinematic region ($10^{-4} < x < 10^{-1}$). The access to the gluon distributions is possible through the study of heavy-flavour production, which, in high-energy hadronic collisions, is dominantly generated by gluon-gluon interactions (Fig. 17).

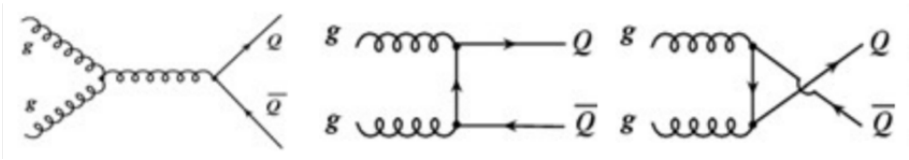

Figure 17: Tree-level Feynman diagrams of heavy-quark pairs production from gluon-gluon interactions in high-energy hadron-hadron collisions.

In general, quarkonium production is extremely valuable to constraint gluon PDFs and nPDFs. Particularly effective probes are the C = +1 quarkonia states. Among these, η_c production has never been studied in high-energy hadron collisions, and its production rate is expected to be substantial at LHCb with SMOG2 [118, 119]. Of particular interest is the investigation of the gluon content of the neutron, as compared to the proton. This can be achieved e.g. by studying J/ψ or Υ production on both H_2 and D_2 targets.

Most of our knowledge about the collinear PDFs comes from decades of inclusive Deep Inelastic Scattering (DIS) experiments. Considering also the explicit dependence of PDFs on the parton transverse momenta (transverse-momentum-dependent PDFs, or TMDs) has opened a radically new perspective in the exploration of the structure of the nucleon (for reviews, see Refs. [120, 121]). Unlike collinear PDFs, which only provide a 1-dimensional description of the nucleon structure in terms of longitudinal momentum fraction of partons, TMDs are sensitive to spin-orbit correlations inside the nucleon. They are thus indirectly sensitive to the still-unknown parton orbital angular momentum, the main missing piece in the proton spin puzzle. In addition, they provide the possibility to map the parton densities in the 3-dimensional momentum space, spanned by the longitudinal momentum fraction x (along the z direction) and by the two transverse momentum components k_x and k_y, allowing for a *nucleon tomography* in momentum space, see Fig. 18. More generally, the knowledge of TMDs will lead to a significantly more profound and fundamental understanding of the complex dynamics of quarks and gluons

in the non-perturbative regime of QCD.

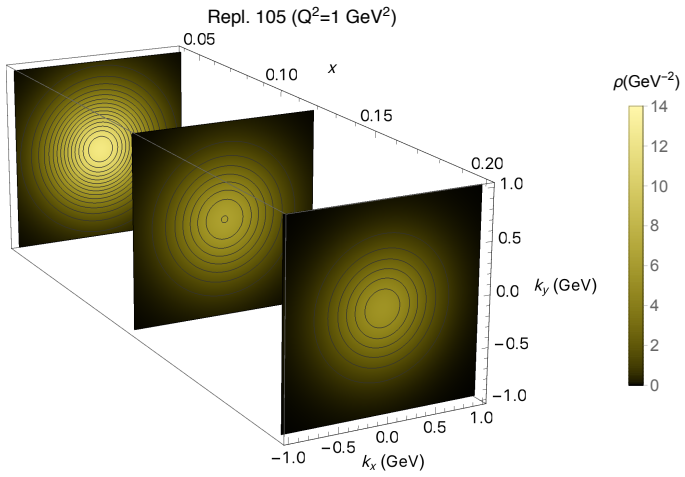

Figure 18: Three-dimensional representation of the u-quark densities in momentum space (proton tomography) from a recent global analysis [122]. (Courtesy of A. Bacchetta).

Two quark TMDs are involved in unpolarized processes: the standard unpolarized distribution function f_1^q and the Boer-Mulders function $h_1^{\perp,q}$ [123]. Even if it requires no target polarization, the Boer-Mulders function is in fact a polarized TMD because it depends on the quark transverse polarization. More specifically, it describes the correlation between the quark transverse polarization and transverse momentum. It is noteworthy that this correlation results in specific azimuthal modulations of the unpolarized cross-section.

In the last 15 years, significant progresses have been achieved in the comprehension of the quark TMDs in Semi-Inclusive DIS (SIDIS) experiments (Hermes, Compass, JLAB) [124]. High-energy pp collisions constitute a complementary approach. In particular, fixed-target pp collisions at the LHC, with a beam energy at the TeV scale, will give access to these objects for unique kinematic conditions (high x, at moderately high Q^2). Furthermore, by comparing the results obtained in SIDIS with those from hadronic collisions, it is possible to perform stringent tests of QCD factorization, evolution and universality. For instance, the Boer-Mulders function mentioned above has the peculiar property of being naive-T-odd. This implies that its definition must include a proper gauge-link (Wilson line) that manifests in a soft-gluon exchange between the ejected quark and the color field of the nucleon remnant. In general, gauge links are process-dependent and this leads to the remarkable fact that naive-T-odd TMDs (such the Boer-Mulders and the Sivers functions) are not universal. In particular, they are expected to have opposite sign when measured in Drell-Yan and SIDIS processes [125]. A solid experimental verification of this direct QCD prediction is eagerly awaited.

At LHCb, the quark f_1^q and $h_1^{\perp,q}$ TMDs can be probed in Drell-Yan processes, exploiting the excellent reconstruction capabilities for muon-pairs. The unpolarized Drell-Yan cross-section can be written as

$$\sigma_{UU}^{DY} \propto A\ f_1^q \otimes f_1^{\bar{q}} + B\ h_1^{\perp,q} \otimes h_1^{\perp,\bar{q}} \cos 2\phi\ , \tag{1}$$

where the subscript UU denotes that both beam and target are unpolarized, the symbol $\otimes$ indicates a convolution integral over the quark transverse momenta, and ϕ is the azimuthal

angle of the final-state di-lepton. By feeding the SMOG2 system with either H_2 and D_2 one can get sensitivity to both the u and d quark contributions.

As mentioned before, another important reason to study unpolarized Drell-Yan processes is to get access to the antiquark content of the nucleon. More specifically, by using H_2 and D_2 targets with SMOG2, one can access the poorly constrained antiquark momentum distributions $\bar{u}(x)$ and $\bar{d}(x)$, complementing the forthcoming E906 results. This is a particularly interesting measurement, since previous experiments have demonstrated that the momentum distributions of $\bar{u}$ and $\bar{d}$ in the proton are very different i.e., against naive expectations, the proton sea is not flavour symmetric (Fig. 19).

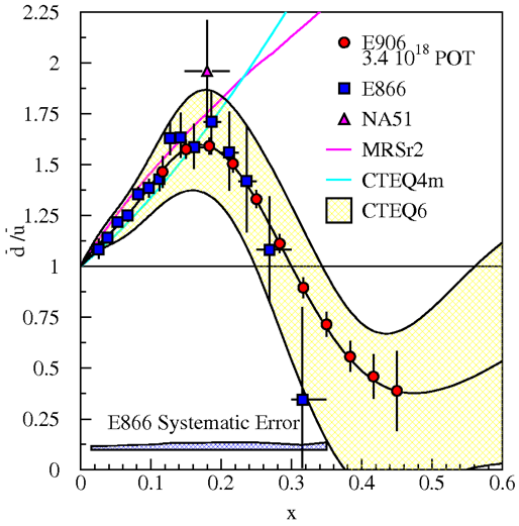

Figure 19: Ratio of $\bar{u}(x)$ and $\bar{d}(x)$ momentum distributions from previous experiments and E906 projected results.

In contrast to the quark TMDs, the present knowledge of the gluon TMDs is very poor. Although the theory framework is well established, experimental information is still extremely limited. Similarly to the quark case, two gluon TMDs appear in unpolarized observables: the spin-independent function f_1^g and the linearly polarized gluon TMD $h_1^{\perp,g}$. The latter is particularly interesting since, analogous to the Boer-Mulders function, it carries information on the gluon (linear) polarization in an unpolarized proton, provided that the intrinsic transverse momentum is not integrated out. Both distribution functions are process dependent [126] and can thus provide stringent tests of QCD universality when compared to the analogous objects measured in ep collisions, e.g. at a future Electron Ion Collider.

As mentioned above, the most efficient way to access the gluon dynamics inside the proton is by measuring suitable heavy-flavour observables. Inclusive quarkonia production in fixed-target pp interactions turns out to be an ideal observable to access the gluon TMDs (Fig. 20).
Since, however, transverse-momentum-dependent QCD factorization requires $p_T(Q) \ll M_Q$, where Q denotes an heavy quark, the most interesting processes to be studied with a H_2 target are back-to-back production of a quarkonium state and an isolated photon, e.g.:

$$pp \to J/\psi + \gamma + X, \quad pp \to \psi' + \gamma + X, \quad pp \to \Upsilon + \gamma + X, \quad \text{etc.}, \tag{2}$$

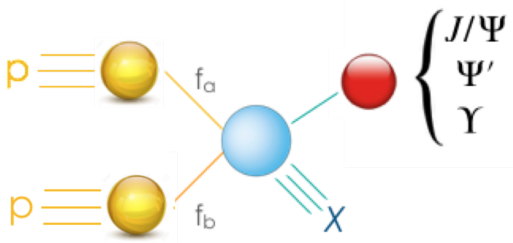

Figure 20: Inclusive quarkonia production in unpolarized pp collisions.

or associated quarkonia production, e.g.:

$$pp \to J/\psi + J/\psi + X, \quad pp \to J/\psi + \psi' + X, \quad pp \to \Upsilon + \Upsilon + X, \quad \text{etc.}, \tag{3}$$

where only the relative p_T has to be small compared to M_Q. The relevant gluon TMDs can be extracted by exploiting the azimuthal dependence of the unpolarized cross-section, where three contributions can be identified at leading order:

$$d\sigma_{UU}^{incl\ Q\bar{Q}} \propto A\ f_1^g \otimes f_1^g + B\ f_1^g \otimes h_1^{\perp,g} \cos 2\phi + C\ h_1^{\perp,g} \otimes h_1^{\perp,g} \cos 4\phi\ . \tag{4}$$

Here the symbol $\otimes$ indicates a convolution integral over the transverse momenta of the gluon and ϕ is the azimuthal angle of the quarkonia+photon system or of the two quarkonia states (associated quarkonia production).

7.1 Worldwide Context

With respect to existing fixed-target facilities at lower energy (SPS, JLAB), SMOG2 will access a novel kinematic region with unique production rates for Drell Yan and heavy flavour final states. An extension of this program has been proposed [12] for future runs, consisting of a polarised target similar to the one used in Hermes [127]. This would provide a rich spin-physics program from hadron collisions, highly complementary to the program at the electron-ion collider, which is proposed on a comparable time scale.

8 Conclusions

During LHC Run 2, the LHCb collaboration has demonstrated the capability to exploit the LHC beams and the LHCb-specific detector capabilities with fixed-target configuration. Production measurements were performed with different collision systems at unprecedented energies for fixed-target experiments, providing novel inputs to nuclear and cosmic-ray physics. Clean samples of charmed hadrons and light charged particles (positively indentified by the PID subdetectors) could be obtained, and absolute cross-sections could be measured with a relative precision better than 10%.

The upgrade of the gas target is expected to boost this program by allowing a wider choice of usable gas species, better control over the target gas pressure, and to increase the integrated luminosities of the fixed-target samples by at least two orders of magnitude. In particular, the use of hydrogen and deuterium will provide a reference for all measurements with heavier nuclei and will allow measurements of the nucleon structure

in a novel kinematic regime. Heavier targets as Xenon can extend the studies of nuclear matter in a domain where QGP effects are expected to be manifest. Further inputs to the modeling of cosmic interactions in the interstellar medium and in the atmosphere can be provided by the use of hydrogen, helium, nitrogen and oxygen targets.

References

[1] S. J. Brodsky, F. Fleuret, C. Hadjidakis, and J. P. Lansberg, *Physics Opportunities of a Fixed-Target Experiment using the LHC Beams*, Phys. Rept. **522** (2013) 239, arXiv:1202.6585.

[2] J. P. Lansberg *et al.*, *Physics at a Fixed-Target Experiment Using the LHC Beams*, Adv. High Energy Phys. **2015** (2015) , Special Issue.

[3] C. Hadjidakis *et al.*, *A Fixed-Target Programme at the LHC: Physics Case and Projected Performances for Heavy-Ion, Hadron, Spin and Astroparticle Studies*, arXiv:1807.00603.

[4] C. Barschel, *Precision luminosity measurement at LHCb with beam-gas imaging*, PhD thesis, RWTH Aachen U., 2014, CERN-THESIS-2013-301.

[5] M. Ferro-Luzzi, *Proposal for an absolute luminosity determination in colliding beam experiments using vertex detection of beam-gas interactions*, Nucl. Instrum. Meth. **A553** (2005) 388.

[6] LHCb collaboration, R. Aaij *et al.*, *Precision luminosity measurements at LHCb*, JINST **9** (2014) P12005, arXiv:1410.0149.

[7] LHCb collaboration, *First look at the pPb pilot run*, LHCb-CONF-2012-034.

[8] LHCb collaboration, A. A. Alves Jr. *et al.*, *The LHCb detector at the LHC*, JINST **3** (2008) S08005.

[9] LHCb collaboration, R. Aaij *et al.*, *LHCb detector performance*, Int. J. Mod. Phys. **A30** (2015) 1530022, arXiv:1412.6352.

[10] LHCb collaboration, *Framework TDR for the LHCb Upgrade: Technical Design Report*, CERN-LHCC-2012-007.

[11] LHCb collaboration, *LHCb VELO Upgrade Technical Design Report*, CERN-LHCC-2013-021.

[12] P. Di Nezza *et al.*, *The SMOG2 and polarised gas target proposal*, Physics Beyond Colliders QCD Working Group Meeting, March 2nd, 2018.

[13] V. Carassiti *et al.*, *SMOG2 Technical Proposal*, tech. rep. in preparation.

[14] UA9 Collaboration, L. Burmistrov *et al.*, *Measurement of Short Living Baryon Magnetic Moment using Bent Crystals at SPS and LHC*, CERN-SPSC-2016-030. SPSC-EOI-012, Jun, 2016.

[15] F. J. Botella *et al.*, *On the search for the electric dipole moment of strange and charm baryons at LHC*, Eur. Phys. J. **C77** (2017) 181, arXiv:1612.06769.

[16] A. S. Fomin *et al.*, *Feasibility of measuring the magnetic dipole moments of the charm baryons at the LHC using bent crystals*, JHEP **08** (2017) 120, arXiv:1705.03382.

[17] E. Bagli *et al.*, *Electromagnetic dipole moments of charged baryons with bent crystals at the LHC*, Eur. Phys. J. **C77** (2017) 828, arXiv:1708.08483.

[18] A. S. Fomin *et al.*, *Feasibility of τ lepton electromagnetic dipole moments measurement using bent crystal at the LHC*, arXiv:1810.06699.

[19] J. Fu *et al.*, *Novel method for the direct measurement of the tau lepton dipole moments*, arXiv:1901.04003.

[20] V. Pugatch, *Physics and Techniques of the Fixed Metal Microstrip Target for the LHCb Experiment. International Conference "CERN-Ukraine co-operation: current state and prospects*, .

[21] LHCb collaboration, R. Aaij *et al.*, *Measurement of antiproton production in pHe collisions at $\sqrt{s_{\rm NN}} = 110$ GeV*, Phys. Rev. Lett. **121** (2018) 222001, arXiv:1808.06127.

[22] LHCb collaboration, R. Aaij *et al.*, *First measurement of charm production fixed-target configuration at the LHC*, arXiv:1810.07907, submitted to Phys. Rev. Lett.

[23] S. Redaelli, M. Ferro-Luzzi, and C. Hadjidakis, *Report from the LHC Fixed Target working group of the CERN Physics Beyond Colliders forum*, tech. rep., Mar, 2019.

[24] T. Matsui and H. Satz, *J/ψ Suppression by Quark-Gluon Plasma Formation*, Phys. Lett. **B178** (1986) 416.

[25] F. Karsch, D. Kharzeev, and H. Satz, *Sequential charmonium dissociation*, Phys. Lett. **B637** (2006) 75, arXiv:hep-ph/0512239.

[26] D. F. Geesaman, K. Saito, and A. W. Thomas, *The nuclear EMC effect*, Ann. Rev. Nucl. Part. Sci. **45** (1995) 337.

[27] J. L. Albacete and C. Marquet, *Gluon saturation and initial conditions for relativistic heavy ion collisions*, Prog. Part. Nucl. Phys. **76** (2014) 1, arXiv:1401.4866.

[28] F. Arleo and S. Peigne, *J/ψ suppression in p-A collisions from parton energy loss in cold QCD matter*, Phys. Rev. Lett. **109** (2012) 122301, arXiv:1204.4609.

[29] A. Capella *et al.*, *Nuclear Effects in J/ψ Suppression*, Phys. Lett. **B206** (1988) 354.

[30] R. Vogt, *Are the J/ψ and χ_c A dependencies the same?*, Nucl. Phys. **A700** (2002) 539, arXiv:hep-ph/0107045.

[31] S. Gavin and R. Vogt, *Charmonium suppression by Comover scattering in Pb + Pb collisions*, Phys. Rev. Lett. **78** (1997) 1006, arXiv:hep-ph/9606460.

[32] A. Capella, A. Kaidalov, A. Kouider Akil, and C. Gerschel, *J/ψ and ψ' suppression in heavy ion collisions*, Phys. Lett. **B393** (1997) 431, arXiv:hep-ph/9607265.

[33] P. Braun-Munzinger and J. Stachel, *(Non)thermal aspects of charmonium production and a new look at J/ψ suppression*, Phys. Lett. **B490** (2000) 196, arXiv:nucl-th/0007059.

[34] Z. Conesa del Valle *et al.*, *Quarkonium production in high energy proton-proton and proton-nucleus collisions*, Nucl. Phys. Proc. Suppl. **214** (2011) 3, arXiv:1105.4545.

[35] LHCb collaboration, R. Aaij *et al.*, *Study of J/ψ production and cold nuclear matter effects in pPb collisions at* $\sqrt{s_{\rm NN}} = 5$ *TeV*, JHEP **02** (2014) 072, arXiv:1308.6729.

[36] LHCb collaboration, R. Aaij *et al.*, *Study of Υ production and cold nuclear matter effects in pPb collisions at* $\sqrt{s_{\rm NN}} = 5$ *TeV*, JHEP **07** (2014) 094, arXiv:1405.5152.

[37] LHCb collaboration, R. Aaij *et al.*, *Study of $\psi(2S)$ production cross-sections and cold nuclear matter effects in pPb collisions at* $\sqrt{s_{\rm NN}} = 5$ *TeV*, JHEP **03** (2016) 133, arXiv:1601.07878.

[38] LHCb collaboration, R. Aaij *et al.*, *Prompt and nonprompt J/ψ production and nuclear modification in pPb collisions at* $\sqrt{s_{\rm NN}} = 8.16$ *TeV*, Phys. Lett. **B774** (2017) 159, arXiv:1706.07122.

[39] LHCb collaboration, R. Aaij *et al.*, *Study of prompt D^0 meson production in pPb collisions at* $\sqrt{s_{\rm NN}} = 5$ *TeV*, JHEP **10** (2017) 090, arXiv:1707.02750.

[40] LHCb collaboration, R. Aaij *et al.*, *Prompt Λ_c^+ production in pPb collisions at* $\sqrt{s_{\rm NN}} = 5.02$ *TeV*, arXiv:1809.01404, accepted for publication in JHEP.

[41] LHCb collaboration, R. Aaij *et al.*, *Study of Υ production in pPb collisions at* $\sqrt{s_{\rm NN}} = 8.16$ *TeV*, JHEP **11** (2018) 194, arXiv:1810.07655.

[42] K. J. Eskola, P. Paakkinen, H. Paukkunen, and C. A. Salgado, *EPPS16: Nuclear parton distributions with LHC data*, Eur. Phys. J. **C77** (2017) 163, arXiv:1612.05741.

[43] S. J. Brodsky, P. Hoyer, C. Peterson, and N. Sakai, *The Intrinsic Charm of the Proton*, Phys. Lett. **93B** (1980) 451.

[44] S. J. Brodsky *et al.*, *A review of the intrinsic heavy quark content of the nucleon*, Adv. High Energy Phys. **2015** (2015) 231547, arXiv:1504.06287.

[45] V. A. Bednyakov *et al.*, *Searching for intrinsic charm in the proton at the LHC*, Phys. Lett. **B728** (2014) 602, arXiv:1305.3548.

[46] G. Bailas and V. P. Goncalves, *Phenomenological implications of the intrinsic charm in the Z boson production at the LHC*, Eur. Phys. J. **C76** (2016) 105, arXiv:1512.06007.

[47] T. Boettcher, P. Ilten, and M. Williams, *Direct probe of the intrinsic charm content of the proton*, Phys. Rev. **D93** (2016) 074008, arXiv:1512.06666.

[48] A. V. Lipatov, G. I. Lykasov, Yu. Yu. Stepanenko, and V. A. Bednyakov, *Probing proton intrinsic charm in photon or Z boson production accompanied by heavy jets at the LHC*, Phys. Rev. **D94** (2016) 053011, arXiv:1606.04882.

[49] ALICE collaboration, J. Adam *et al.*, *D-meson production in p-Pb collisions at* $\sqrt{s_{NN}} = 5.02$ *TeV and in pp collisions at* $\sqrt{s} = 7$ *TeV*, Phys. Rev. **C94** (2016) 054908, arXiv:1605.07569.

[50] M. L. Mangano *et al.*, *Heavy quark correlations in hadron collisions at next-to-leading order*, Nucl. Phys. **B373** (1992) 295.

[51] J.-P. Lansberg and H.-S. Shao, *Towards an automated tool to evaluate the impact of the nuclear modification of the gluon density on quarkonium, D and B meson production in proton-nucleus collisions*, Eur. Phys. J. **C77** (2017) 1, arXiv:1610.05382.

[52] H.-S. Shao, *HELAC-Onia 2.0: an upgraded matrix-element and event generator for heavy quarkonium physics*, Comput. Phys. Commun. **198** (2016) 238, arXiv:1507.03435.

[53] H.-S. Shao, *HELAC-Onia: An automatic matrix element generator for heavy quarkonium physics*, Comput. Phys. Commun. **184** (2013) 2562, arXiv:1212.5293.

[54] S. Dulat *et al.*, *New parton distribution functions from a global analysis of quantum chromodynamics*, Phys. Rev. **D93** (2016) 033006.

[55] K. Kovarik *et al.*, *nCTEQ15 - Global analysis of nuclear parton distributions with uncertainties in the CTEQ framework*, Phys. Rev. **D93** (2016) 085037.

[56] STAR collaboration, G. Xie, Λ_c *Production in Au+Au Collisions at* $\sqrt{s_{NN}}$ = *200 GeV measured by the STAR experiment*, Nucl. Phys. **A967** (2017) 928, arXiv:1704.04353.

[57] ALICE, S. Acharya *et al.*, Λ_c^+ *production in Pb-Pb collisions at* $\sqrt{s_{\rm NN}} = 5.02$ *TeV*, Submitted to: Phys. Lett. (2018) arXiv:1809.10922.

[58] ALICE, S. Acharya *et al.*, Λ_c^+ *production in pp collisions at* $\sqrt{s} = 7$ *TeV and in p-Pb collisions at* $\sqrt{s_{\rm NN}} = 5.02$ *TeV*, JHEP **04** (2018) 108, arXiv:1712.09581.

[59] LHCb collaboration, R. Aaij *et al.*, *Forward production of* Υ *mesons in pp collisions at* $\sqrt{s} = 7$ *and* 8 *TeV*, JHEP **11** (2015) 103, arXiv:1509.02372.

[60] T. Sjöstrand, S. Mrenna, and P. Skands, *A brief introduction to PYTHIA 8.1*, Comput. Phys. Commun. **178** (2008) 852, arXiv:0710.3820.

[61] LHCb collaboration, *Inclusive low mass Drell-Yan production in the forward region at* $\sqrt{s} = 7$ *TeV*, LHCb-CONF-2012-013.

[62] H. Song and U. W. Heinz, *Causal viscous hydrodynamics in 2+1 dimensions for relativistic heavy-ion collisions*, Phys. Rev. **C77** (2008) 064901, arXiv:0712.3715.

[63] B. Schenke, S. Jeon, and C. Gale, *Elliptic and triangular flow in event-by-event (3+1)D viscous hydrodynamics*, Phys. Rev. Lett. **106** (2011) 042301, arXiv:1009.3244.

[64] I. A. Karpenko, P. Huovinen, H. Petersen, and M. Bleicher, *Estimation of the shear viscosity at finite net-baryon density from* $A + A$ *collision data at* $\sqrt{s_{\rm NN}} = 7.7 - 200$ *GeV*, Phys. Rev. **C91** (2015) 064901, arXiv:1502.01978.

[65] C. Shen and B. Schenke, *Dynamical initial state model for relativistic heavy-ion collisions*, Phys. Rev. **C97** (2018) 024907, arXiv:1710.00881.

[66] M. A. Stephanov, *QCD phase diagram and the critical point*, Prog. Theor. Phys. Suppl. **153** (2004) 139, arXiv:hep-ph/0402115.

[67] X. Luo and N. Xu, *Search for the QCD Critical Point with Fluctuations of Conserved Quantities in Relativistic Heavy-Ion Collisions at RHIC : An Overview*, Nucl. Sci. Tech. **28** (2017) 112, arXiv:1701.02105.

[68] CMS collaboration, V. Khachatryan *et al.*, *Observation of Long-Range Near-Side Angular Correlations in Proton-Proton Collisions at the LHC*, JHEP **09** (2010) 091, arXiv:1009.4122.

[69] CMS collaboration, S. Chatrchyan *et al.*, *Observation of long-range near-side angular correlations in proton-lead collisions at the LHC*, Phys. Lett. **B718** (2013) 795, arXiv:1210.5482.

[70] ALICE collaboration, B. Abelev *et al.*, *Long-range angular correlations on the near and away side in p-Pb collisions at* $\sqrt{s_{NN}} = 5.02$ *TeV*, Phys. Lett. **B719** (2013) 29, arXiv:1212.2001.

[71] ATLAS collaboration, G. Aad *et al.*, *Observation of Associated Near-Side and Away-Side Long-Range Correlations in* $\sqrt{s_{NN}}$*=5.02TeV Proton-Lead Collisions with the ATLAS Detector*, Phys. Rev. Lett. **110** (2013) 182302, arXiv:1212.5198.

[72] LHCb collaboration, R. Aaij *et al.*, *Measurements of long-range near-side angular correlations in* $\sqrt{s_{NN}} = 5\,TeV$ *proton-lead collisions in the forward region*, Phys. Lett. **B762** (2016) 473, arXiv:1512.00439.

[73] PHENIX collaboration, A. Adare *et al.*, *Pseudorapidity Dependence of Particle Production and Elliptic Flow in Asymmetric Nuclear Collisions of p+Al, p+Au, d+Au, and* ^{3}*He+Au at* $\sqrt{s_{NN}} = 200$ *GeV*, Phys. Rev. Lett. **121** (2018) 222301, arXiv:1807.11928.

[74] LHCb collaboration, R. Aaij *et al.*, *Updated measurements of exclusive J/*ψ *and* $\psi(2S)$ *production cross-sections in pp collisions at* $\sqrt{s} = 7$ *TeV*, J. Phys. **G41** (2014) 055002, arXiv:1401.3288.

[75] LHCb collaboration, R. Aaij *et al.*, *Central exclusive production of J/*ψ *and* $\psi(2S)$ *mesons in pp collisions at* $\sqrt{s} = 13$ *TeV*, JHEP **10** (2018) 167, arXiv:1806.04079.

[76] LHCb collaboration, R. Aaij *et al.*, *Measurement of the exclusive* $\Upsilon(nS)$ *production cross-section in pp collisions at* $\sqrt{s} = 7$ *TeV and* 8 *TeV*, JHEP **09** (2015) 084, arXiv:1505.08139.

[77] LHCb collaboration, *Study of coherent production of J/*ψ *in lead-lead collisions at* $\sqrt{s_{NN}} = 5$ *TeV with the LHCb experiment*, LHCb-CONF-2018-003.

[78] V. P. Goncalves and W. K. Sauter, η_c *production in photon-induced interactions at a fixed target experiment at LHC as a probe of the odderon*, Phys. Rev. **D91** (2015) 094014, arXiv:1503.05112.

[79] S. R. Klein, *Comment on "*η_c *production in photon-induced interactions at the LHC"*, Phys. Rev. **D98** (2018) 118501, arXiv:1808.08253.

[80] V. P. Gonalves and M. M. Jaime, *Exclusive vector meson photoproduction in fixed - target collisions at the LHC*, Eur. Phys. J. **C78** (2018) 693, arXiv:1802.04713.

[81] STAR collaboration, L. Adamczyk *et al.*, *Global Λ hyperon polarization in nuclear collisions: evidence for the most vortical fluid*, Nature **548** (2017) 62, arXiv:1701.06657.

[82] F. Becattini, L. Csernai, and D. J. Wang, Λ *polarization in peripheral heavy ion collisions*, Phys. Rev. **C88** (2013) 034905, arXiv:1304.4427, [Erratum: Phys. Rev.C93,no.6,069901(2016)].

[83] PAMELA collaboration, V. Bonvicini *et al.*, *The PAMELA experiment in space*, Nucl. Instrum. Meth. **A461** (2001) 262.

[84] A. Kounine, *The Alpha Magnetic Spectrometer on the International Space Station*, Int. J. Mod. Phys. **E21** (2012) 1230005.

[85] G. Giesen *et al.*, *AMS-02 antiprotons, at last! Secondary astrophysical component and immediate implications for Dark Matter*, JCAP **09** (2015) 023, arXiv:1504.04276.

[86] M. di Mauro, F. Donato, A. Goudelis, and P. D. Serpico, *New evaluation of the antiproton production cross section for cosmic ray studies*, Phys. Rev. **D90** (2014) 085017, arXiv:1408.0288.

[87] R. Kappl, A. Reinert, and M. W. Winkler, *AMS-02 Antiprotons Reloaded*, JCAP **10** (2015) 034, arXiv:1506.04145.

[88] NA49 collaboration, T. Anticic *et al.*, *Inclusive production of protons, anti-protons and neutrons in p+p collisions at 158-GeV/c beam momentum*, Eur. Phys. J. **C65** (2010) 9, arXiv:0904.2708.

[89] NA61/SHINE collaboration, A. Aduszkiewicz *et al.*, *Measurements of $\pi^{\pm}$, $K^{\pm}$, p and $\bar{p}$ spectra in proton-proton interactions at 20, 31, 40, 80 and 158 GeV/c with the NA61/SHINE spectrometer at the CERN SPS*, Eur. Phys. J. **C77** (2017) 671, arXiv:1705.02467.

[90] NA49 collaboration, H. G. Fischer, *Baryon yields, isospin effects and strangeness production in elementary hadronic interactions*, Acta Phys. Hung. **A17** (2003) 369.

[91] T. Pierog *et al.*, *EPOS LHC: Test of collective hadronization with data measured at the CERN Large Hadron Collider*, Phys. Rev. **C92** (2015) 034906, arXiv:1306.0121.

[92] T. Pierog and K. Werner, *EPOS Model and Ultra High Energy Cosmic Rays*, Nucl. Phys. Proc. Suppl. **196** (2009) 102, arXiv:0905.1198.

[93] M. Gyulassy and X.-N. Wang, *HIJING 1.0: A Monte Carlo program for parton and particle production in high-energy hadronic and nuclear collisions*, Comput. Phys. Commun. **83** (1994) 307, arXiv:nucl-th/9502021.

[94] M. Kachelriess, I. V. Moskalenko, and S. S. Ostapchenko, *New calculation of antiproton production by cosmic ray protons and nuclei*, Astrophys. J. **803** (2015) 54, arXiv:1502.04158.

[95] GAPS collaboration, T. Aramaki *et al.*, *Antideuteron Sensitivity for the GAPS Experiment*, Astropart. Phys. **74** (2016) 6, arXiv:1506.02513.

[96] T. Aramaki *et al.*, *Review of the theoretical and experimental status of dark matter identification with cosmic-ray antideuterons*, Phys. Rept. **618** (2016) 1, arXiv:1505.07785.

[97] ALICE collaboration, S. Acharya *et al.*, *Production of deuterons, tritons, ^{3}He nuclei and their antinuclei in pp collisions at $\sqrt{s}$ = 0.9, 2.76 and 7 TeV*, Phys. Rev. **C97** (2018) 024615, arXiv:1709.08522.

[98] K.-H. Kampert and M. Unger, *Measurements of the Cosmic Ray Composition with Air Shower Experiments*, Astropart. Phys. **35** (2012) 660, arXiv:1201.0018.

[99] Z. Citron *et al.*, *Future physics opportunities for high-density QCD at the LHC with heavy-ion and proton beams*, in *HL/HE-LHC Workshop: Workshop on the Physics of HL-LHC, and Perspectives at HE-LHC Geneva, Switzerland, June 18-20, 2018*, 2018. arXiv:1812.06772.

[100] R. Ulrich, R. Engel, and M. Unger, *Hadronic Multiparticle Production at Ultra-High Energies and Extensive Air Showers*, Phys. Rev. **D83** (2011) 054026, arXiv:1010.4310.

[101] R. M. Ulrich *et al.*, *The impact of a fixed-target experiment with LHC beam for astroparticle physics*, PoS **ICRC2015** (2016) 407.

[102] IceCube collaboration, M. G. Aartsen *et al.*, *Evidence for High-Energy Extraterrestrial Neutrinos at the IceCube Detector*, Science **342** (2013) 1242856, arXiv:1311.5238.

[103] PROSA collaboration, M. V. Garzelli *et al.*, *Prompt neutrino fluxes in the atmosphere with PROSA parton distribution functions*, JHEP **05** (2017) 004, arXiv:1611.03815.

[104] A. Fedynitch *et al.*, *The hadronic interaction model Sibyll-2.3c and inclusive lepton fluxes*, arXiv:1806.04140.

[105] R. Laha and S. J. Brodsky, *IceCube can constrain the intrinsic charm of the proton*, Phys. Rev. **D96** (2017) 123002, arXiv:1607.08240.

[106] IceCube collaboration, M. G. Aartsen *et al.*, *Measurement of the Atmospheric ν_e Spectrum with IceCube*, Phys. Rev. **D91** (2015) 122004, arXiv:1504.03753.

[107] IceCube collaboration, M. G. Aartsen *et al.*, *The IceCube Neutrino Observatory - Contributions to ICRC 2015 Part II: Atmospheric and Astrophysical Diffuse Neutrino Searches of All Flavors*, in *Proceedings, 34th International Cosmic Ray Conference (ICRC 2015): The Hague, The Netherlands, July 30-August 6, 2015*, 2015. arXiv:1510.05223.

[108] H. P. Dembinski *et al.*, *Report on tests and measurements of hadronic interaction properties with air showers*, UHECR 2018 conference, 2018. Paris, France.

[109] I.C. Maris for the NA61/SHINE Collaboration, *Hadron Production Measurements with the NA61/SHINE Experiment and their Relevance for Air Shower Simulations*, Proceedings, 31th International Cosmic Ray Conference (ICRC 2009), 2009.

[110] S. Ostapchenko, *Monte Carlo treatment of hadronic interactions in enhanced Pomeron scheme: I. QGSJET-II model*, Phys. Rev. **D83** (2011) 014018, arXiv:1010.1869.

[111] R. S. Fletcher, T. K. Gaisser, P. Lipari, and T. Stanev, *SIBYLL: An Event generator for simulation of high-energy cosmic ray cascades*, Phys. Rev. **D50** (1994) 5710.

[112] T. Pierog, C. Baus, and R. Ulrich, *CRMC (Cosmic Ray Monte Carlo package)*, web.ikp.kit.edu/rulrich/crmc.html.

[113] B. Adams *et al.*, *Letter of Intent: A New QCD facility at the M2 beam line of the CERN SPS (COMPASS++/AMBER)*, arXiv:1808.00848.

[114] NNPDF collaboration, R. D. Ball *et al.*, *Parton distributions for the LHC Run II*, JHEP **04** (2015) 040, arXiv:1410.8849.

[115] A. Accardi *et al.*, *Constraints on large-x parton distributions from new weak boson production and deep-inelastic scattering data*, Phys. Rev. **D93** (2016) 114017, arXiv:1602.03154.

[116] T. Jezo *et al.*, *NLO+NLL limits on W' and Z' gauge boson masses in general extensions of the Standard Model*, JHEP **12** (2014) 092, arXiv:1410.4692.

[117] P. Jimenez-Delgado and E. Reya, *Delineating parton distributions and the strong coupling*, Phys. Rev. **D89** (2014) 074049, arXiv:1403.1852.

[118] LHCb collaboration, R. Aaij *et al.*, *Measurement of the ratio of prompt χ_c to J/ψ production in pp collisions at $\sqrt{s} = 7$ TeV*, Phys. Lett. **B718** (2012) 431, arXiv:1204.1462.

[119] R. Gauld and J. Rojo, *Precision determination of the small-x gluon from charm production at LHCb*, Phys. Rev. Lett. **118** (2017) 072001, arXiv:1610.09373.

[120] V. Barone, F. Bradamante, and A. Martin, *Transverse-spin and transverse-momentum effects in high-energy processes*, Prog. Part. Nucl. Phys. **65** (2010) 267, arXiv:1011.0909.

[121] C. A. Aidala, S. D. Bass, D. Hasch, and G. K. Mallot, *The Spin Structure of the Nucleon*, Rev. Mod. Phys. **85** (2013) 655, arXiv:1209.2803.

[122] A. Bacchetta *et al.*, *Extraction of partonic transverse momentum distributions from semi-inclusive deep-inelastic scattering, Drell-Yan and Z-boson production*, JHEP **06** (2017) 081, arXiv:1703.10157.

[123] D. Boer and P. J. Mulders, *Time reversal odd distribution functions in leptoproduction*, Phys. Rev. **D57** (1998) 5780, arXiv:hep-ph/9711485.

[124] H. Avakian, A. Bressan, and M. Contalbrigo, *Experimental results on TMDs*, Eur. Phys. J. **A52** (2016) 150, [Erratum: Eur. Phys. J.A52,no.6,165(2016)].

[125] J. C. Collins, *Leading twist single transverse-spin asymmetries: Drell-Yan and deep inelastic scattering*, Phys. Lett. **B536** (2002) 43, arXiv:hep-ph/0204004.

[126] D. Boer, *Gluon TMDs in quarkonium production*, Few Body Syst. **58** (2017) 32, arXiv:1611.06089.

[127] HERMES collaboration, A. Airapetian *et al.*, *The HERMES polarized hydrogen and deuterium gas target in the HERA electron storage ring*, Nucl. Instrum. Meth. **A540** (2005) 68, arXiv:physics/0408137.